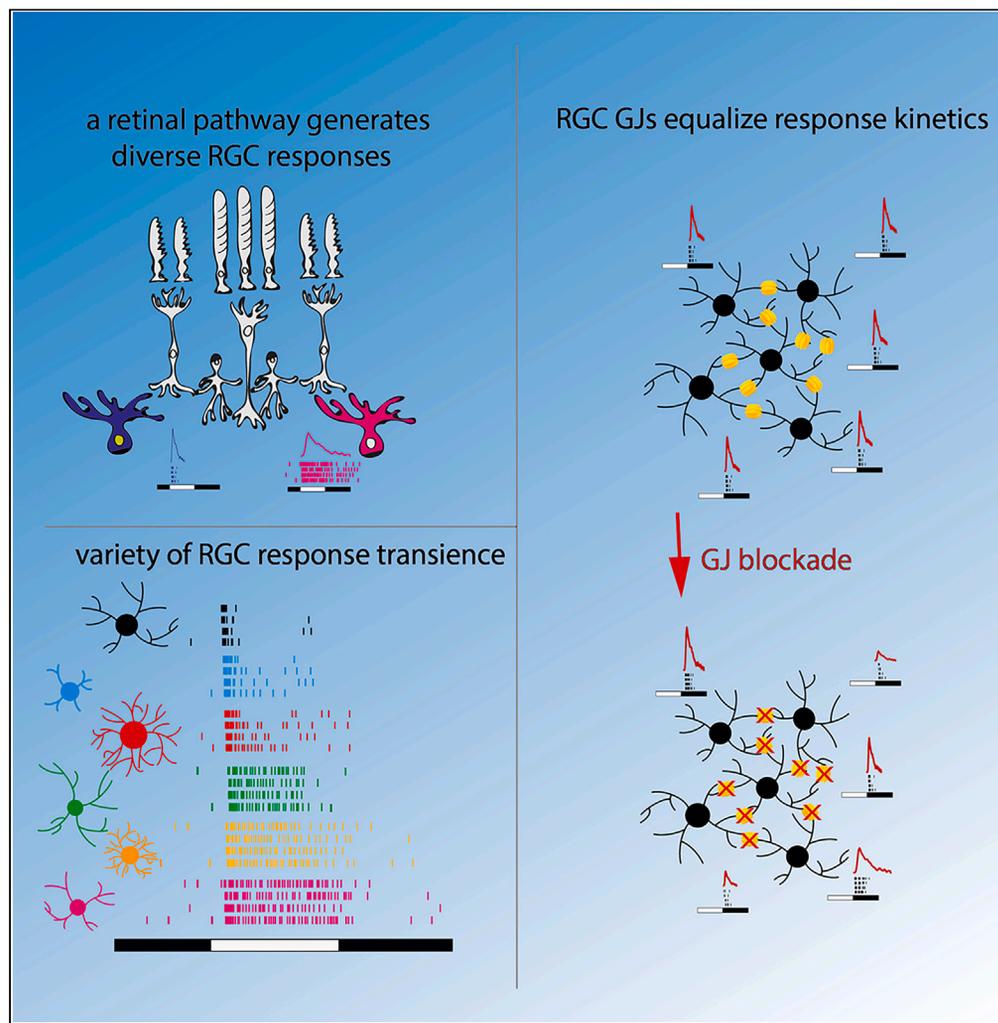**Article**

Gap junctions fine-tune ganglion cell signals to equalize response kinetics within a given electrically coupled array

Gergely Szarka,
Alma Ganczer,
Márton Balogh, ...,
Feng Pan, Tamás
Kovács-Öller, Béla
Völgyi

volgyibela@gmail.com

Highlights

RGC response transience
values form a continuum

A single retinal pathway
carries signals to both
sustained and transient
RGCs

GJ mediated lateral
excitation fine-tunes RGC
response kinetics

tOFFα RGC GJs equalize
kinetic features for cells in
the coupled array

Article

Gap junctions fine-tune ganglion cell signals to equalize response kinetics within a given electrically coupled array

Gergely Szarka,[1,2,3,4,5] Alma Ganczer,[1,2,3,4] Márton Balogh,[1,2,3,4] Ádám Jonatán Tengölics,[1,2,3,4]
Anett Futácsi,[1,3,4,5] Garrett Kenyon,[6] Feng Pan,[7] Tamás Kovács-Öller,[1,2,3,4,5] and Béla Völgyi[1,2,3,4,8,*]

SUMMARY

Retinal ganglion cells (RGCs) summate inputs and forward a spike train code to the brain in the form of either maintained spiking (sustained) or a quickly decaying brief spike burst (transient). We report diverse response transience values across the RGC population and, contrary to the conventional transient/sustained scheme, responses with intermediary characteristics are the most abundant. Pharmacological tests showed that besides GABAergic inhibition, gap junction (GJ)–mediated excitation also plays a pivotal role in shaping response transience and thus visual coding. More precisely GJs connecting RGCs to nearby amacrine and RGCs play a defining role in the process. These GJs equalize kinetic features, including the response transience of transient OFF alpha (tOFFα) RGCs across a coupled array. We propose that GJs in other coupled neuron ensembles in the brain are also critical in the harmonization of response kinetics to enhance the population code and suit a corresponding task.

INTRODUCTION

Information gathered from the visual field travels through parallel intraretinal pathways and converges onto retinal ganglion cells (RGCs) that, in turn, summate and encrypt incoming signals into action potential trains prior to transmitting the signal toward the brain. Light-evoked RGC responses have been previously characterized by their polarity (ON, OFF, and ON-OFF), their sensitivity to various stimuli, and their response kinetics. Based on response speed, RGCs can be sorted into either brisk or sluggish categories, whereas spiking patterns can be maintained (sustained) or a brisk burst (transient). Both aspects of RGC response kinetics are important in terms of signal efficiency on postsynaptic neuronal targets in higher visual centers.[1–3] The aforementioned transient/sustained dichotomy of the spiking activity has been documented in a variety of vertebrate species, including cold-blooded animals, primates, and non-primate mammals.[4–14] Since all photoreceptors generate sustained responses upon illumination,[15] a sustained-to-transient response transformation must occur at some point along the retinal signal flow. Previous work in the salamander and rabbit retinas suggested that response transience is determined by the kinetics of the glutamate receptors (mGluR$_6$, AMPA, Kainate) at the site of the very first retinal contact, the photoreceptor-to-bipolar cell synapse.[16,17] In contrast, more recent studies presented evidence for multiple sites of retinal circuitry that may participate in determining response transience.[18–20] According to these reports, RGCs use diverse mechanisms to produce sustained or transient light responses in a subtype dependent manner and outer retinal postsynaptic receptor (AMPA/kainate receptor) desensitization exerts only a minor effect on response transience. Moreover, the contribution of inner retinal GABAergic inhibition to shape RGC response kinetics has been shown repeatedly,[11,21–26] suggesting that inner retinal pathways likely play a non-negligible role in shaping transience. It has also been reported that gap junction (GJ)-mediated excitatory inputs contribute to various response components of electrically coupled ON direction selective (ON DS) and OFF alpha RGCs.[27–29] In addition, the population of intrinsically photosensitive RGCs (ipRGC) has been shown to pass signals to electrically coupled amacrine cells, thereby modifying their response kinetics.[30] On the other hand, it is not well known how exactly excitatory GJ signaling affects RGC response kinetics and if this is a general phenomenon across the RGC population.

To this end, we performed a combination of morphological analyses, extracellular RGC spike recordings, Ca^{++}-imaging and pharmacological treatments in the mouse retina to study how RGC GJs fine-tune the light response kinetics prior to conveying information toward visual brain centers. In this paper, we present data showing that most RGCs display intermediary (neither transient nor sustained) full field light

[1]University of Pécs, Szentágothai Research Centre, Pécs, Hungary
[2]University of Pécs, Department of Neurobiology, Pécs, Hungary
[3]MTA-PTE NAP 2 Retinal Electrical Synapses Research Group, Pécs, Hungary
[4]Center for Neuroscience, University of Pécs, Pécs, Hungary
[5]SzKK Imaging Core Facility, Szentágothai Research Centre, University of Pécs, Pécs, Hungary
[6]Los Alamos National Laboratory, Los Alamos, NM, USA
[7]The Hong Kong Polytechnic University, Hong Kong, China
[8]Lead contact
*Correspondence: volgyibela@gmail.com
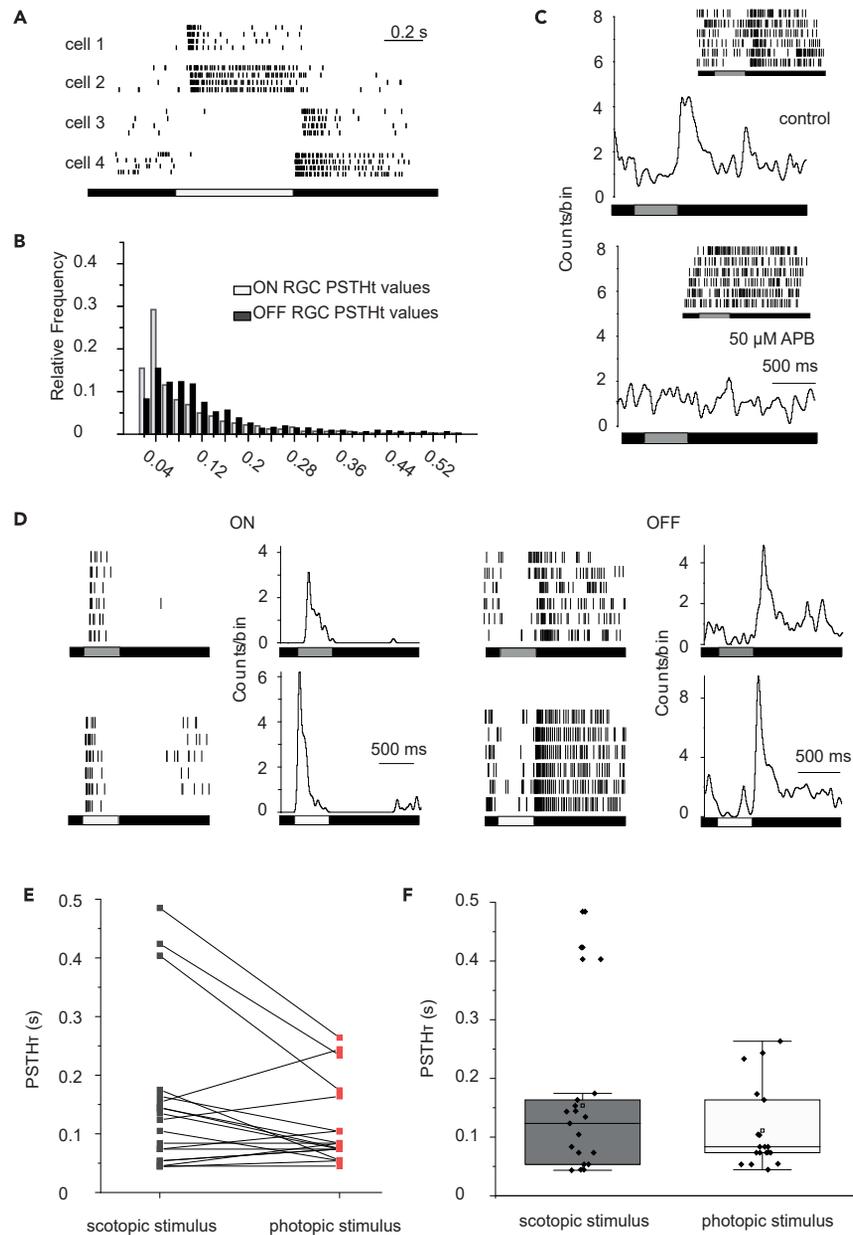https://doi.org/10.1016/j.isci.2024.110099

Figure 1. Scotopic and photopic light response transience of mouse RGCs

(A) Perievent rasters show the light responses of two ON (top two panels; cell# 1 and 2) and two OFF (bottom two panels; cell# 3 and 4) RGCs evoked by a photopic, homogeneous, full-field light stimulus. The horizontal bar on the bottom represents the on- (white) and offset (black) of the stimulus; each recording represents 4 trials of the same cell. For both the ON- and the OFF subpopulations, transient (cell 1 and 3) and sustained (cell 2 and 4) responses were present as well.

(B) Frequency histogram showing the relative abundance of RGC transience (PSTHτ) values for the ON (white) and OFF (black) RGC subpopulations (see the STAR methods sections for PSTHτ calculations). The histogram displays a wide range for both ON- (white) and OFF (black) transience values but fails to clearly separate transient and sustained RGC populations, due to the presence of numerous cells with intermediate response kinetics.

(C) Panels show PSTHs and corresponding peristimulus rasters (six trials of the same RGC) for an OFF RGC under control conditions (top panel) and for the same RGC following an APB (50 μM) treatment while the retina was stimulated by scotopic stimuli. Horizontal bars represent the on- (gray) and offset (black) of the scotopic light stimulus. Clearly, the pharmacological intervention deleted all RGC responses attesting that the primary rod pathway carried the corresponding signals.

(D) Representative ON RGC light responses (raster to the left and PSTH to the right for the same RGC) were evoked first by scotopic (top) and then photopic (bottom) full-field light stimuli. This change in the stimulus strength induced a clear alteration of the response amplitude but the overall shape (response delay and decay) of this particular cell remained largely unchanged. Similarly, a representative OFF RGC displays light responses that, besides subtle changes in response amplitude, appear similar in scotopic (top) and photopic (bottom) stimulating conditions.

Figure 1. *Continued*

(E) Diagram displays PSTHτ value pairs for individual RGC light responses in scotopic (black) and photopic (red) light stimulations. Clearly, the change in stimulus strength induced the alteration of PSTHτ values for many examined RGCs, however, the overall range of response transience values for the entire RGC population were comparable (or greater) in scotopic conditions than those obtained with photopic stimulation paradigms.

(F) Floating bar diagrams show a similar variability of RGC response PSTHτ values in both scotopic (gray) and photopic (white) conditions. Shown are mean values (line) , 25% and 75% quartiles (boxes), standard deviation (whiskers).

responses, a finding that necessitates the reconsideration of the previously accepted transient/sustained response dichotomy.[16,17] We also found that a single vertical signaling route can feed signals to both sustained and transient RGCs, inferring that the vertical carrying retinal pathways do not determine RGC response transience. Additionally, according to our findings, the effect of lateral GJ mediated excitation on RGC response transience was as significant as GABAergic inhibitory signals. However, the effects of GJ mediated excitation were heterogeneous in their magnitude and polarity across the entire RGC population as well as the subpopulation that maintains direct GJ coupling to RGC and/or amacrine cell neighbors. Interestingly, the GJ connection altered RGC response transience heterogeneously even when cells of a single RGC subtype, tOFFα RGCs were examined. Finally, we found that neuronal partners of the same coupled tOFFα RGC array utilized GJ mediated lateral excitation to equalize response kinetics, including transience. Our data thus indicate that inner retinal GJs play an essential role in shaping RGC response transience and partake in encoding of various stimulus features.

RESULTS

The primary rod pathway carries signals to both transient and sustained RGCs

The goal of this work was to examine retinal circuit mechanisms underlying sustained and transient RGC responses. To this end we recorded full-field photopic (I = 100 Rh*/rod/s) RGC responses via either MEA or HD-MEA extracellular recording procedures (n = 6). We divided our RGC population into ON (N = 2540) and OFF (N = 1484) polarity cells (ON and OFF response components of ON-OFF RGCs were also used; although this description did not examine separately ON-OFF RGCs, like the ON-OFF DS cell type, but collected information for ON-OFF cells and sorted response components to the corresponding cohort of data). Using these recordings, we generated PSTHs for each response and assigned numerical values expressing response transience using the PSTHτ method[18] (see STAR methods). We found that the mean PSTHτ for the examined ON RGC population was 0.109 s (SD: +/−0. 99) and the values varied considerably covering a range of 0.02–0.598 s (Figures 1A and 1B). In addition, while clear transient and sustained responses were relatively rare, a considerable fraction of cells displayed intermediary response kinetics that could not undoubtedly be categorized either as transient or sustained spiking. Thus, in agreement with our previous observations[19] no sign of a clear transient/sustained division was established based on our present dataset. Instead, PSTHτ values of ON RGCs rather formed a single continuum. Akin to photopic ON cell responses, PSTHτ values of OFF cells varied across a wide range and showed a continuum of transient, sustained, and intermediary responses (Figures 1A and 1B). Although, transient ON RGC responses were somewhat more numerous, which is in agreement with previous descriptions,[31] the overall shape of the ON and OFF RGC frequency histograms were similar (OFF mean: 0.137 s, SD: +/−0.109; range: 0.02–0.592). Clearly, the wide range and the lack of a clear transient/sustained separation of responses due to the numerous intermediate transience cells were features shared by both the ON and OFF RGC populations.

The observed high variety in RGC response transience may reflect the various kinetics by which parallel retinal pathways convey signals from the outer retina to the output RGCs and/or could potentially be the result of various excitatory/inhibitory lateral neuronal interactions in the two plexiform layers. In the first case, regardless of the subtype, all RGCs should maintain comparable response transience when a single bipolar cell type dominates their inputs. Although photopic signals are delivered by 5–6 bipolar cells to ON cell RGCs, low scotopic signals reach RGCs mostly via the primary rod pathway that operates with the single rod bipolar cell type. Similarly, OFF polarity low scotopic signals are also carried by a single rod bipolar cell type toward RGCs, whereas 4–5 cone bipolar cells convey signals from the outer to the inner retina under photopic conditions. Consequently, if bipolar cell signaling is the key factor in determining response transience, then all low scotopic RGC responses should appear similar in terms of their transience. To investigate this, RGCs were presented with low-scotopic stimuli (1–4.6 Rh*/rod/sec), in which condition the cone pathways and the secondary rod pathway are inactive.[32–35] To test if our scotopic stimulus activates the primary rod pathway, whereas alternative scotopic signaling routes remain quiet, OFF RGCs were presented with full-field scotopic stimuli in control conditions and following the application of the mGluR$_6$ agonist (N = 22; APB 50 μM). We found that under these conditions, all OFF RGC responses were diminished with APB (Figure 1C) thus providing evidence that the dominant signaling route was truly the primary rod pathway while the contribution of other signaling routes, including the secondary rod pathway was negligible. Next, we tested a set of RGCs (N = 19) to see if their response kinetics changes considerably when scotopic stimuli are switched to photopic (from 1 to 4.6 Rh*/rod/sec to 100 Rh*/rod/sec). We found that low-scotopic ON and OFF RGC responses, though appeared somewhat more sustained (scotopic mean: 0.155 s, SD 0.134; photopic mean: 0.110 s, SD - 0.091; p = 0.038) varied considerably in terms of their PSTHτ values, similarly to their photopic counterparts (Figures 1D–1F). While PSTHτ values of photopic RGC responses ranged between 0.045 and 0.26 s for the examined RGC population, the range was 0.044–0.485 s for scotopic responses of the same cells. According to our data, the scotopic RGC response transience range in fact was comparable (or even greater) to those observed for photopic responses.

To see how individual RGC response kinetics were altered by the modified light stimulations we compared scotopic and photopic full-field light responses (M = 19). We found that a small fraction of these cells showed little (if any) change (N = 3) or a minor increase (N = 6) of their response transience values, whereas about the half of the population (N = 10) showed decrease of the transience when scotopic stimuli were
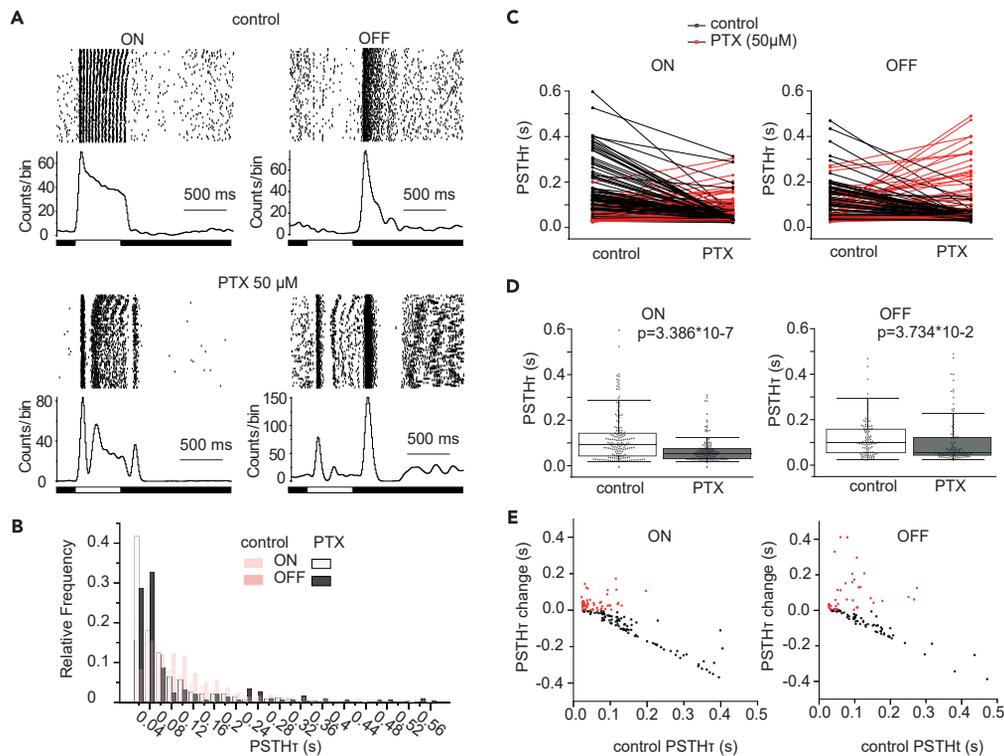
Figure 2. GABA receptor blockade induces abrupt changes in RGC response transience

(A) Representative ON (left) and OFF (right) RGC light responses (rasters at the top and corresponding PSTHs below) are clearly altered when the nonspecific GABA receptor blocker PTX was applied (bottom panels of the same RGCs). The observed changes included the elimination of a sustained response component (shoulder) for the OFF cell and the unmasking of other response components (OFF pathway driven spiking for the ON cell and ON pathway driven spiking of the OFF cell, consistent with previous reports.[27,28,36]

(B) The frequency histograms show that the GABA-A blockade decreased the number of RGCs with intermediary responses and many RGC responses became transient.

(C–E) Apart from a handful of cells showing no considerable change, the GABA receptor blockade induced an overall decrease of PSTHτ values for most examined ON (left) and many OFF (right) RGCs (C). This PTX mediated decrease is also reflected in a drop of mean and median PSTHτ values for both ON (left) and OFF (right) RGC subpopulations ($p < 0.05$, paired t-test). Shown are mean values (line), 25% and 75% quartiles (boxes), standard deviation (whiskers) (D). Scatterplots show that the GABA-A blockade appeared to be more effective on sustained RGC responses that became more transient following drug application (positive dimension reflects a transient-to-sustained, whereas negative dimension reflects a sustained-to-transient change) (E).

replaced with photopic light. Accordingly, the data showed a reduction of the mean (scotopic-to-photopic: 0.154 s–0.112 s), the standard deviation (scotopic-to-photopic: 0.134 s–0.069 s), the median (scotopic-to-photopic: 0.124 s–0.084 s) as well as the range (scotopic-to-photopic: 0.044 s–0.485 s to 0.045 s–0.264 s) of RGC transience values. The changes observed for the mean transience values appeared significant (paired t-test; $p = 0.15*10^{-3}$). A further observation was that transient scotopic responses appeared more resistant to the change while those displaying sustained scotopic responses tended to attain more transient characteristics when photopic light stimuli were presented (Figure 1E). Although the presented data show that certain RGCs provide somewhat more sustained responses under scotopic conditions, the sole primary scotopic pathway clearly serves signaling to both transient and sustained RGCs. Therefore, RGC signal kinetics are not simply inherited from presynaptic bipolar cells, but incoming signals rather undergo additional changes. Therefore, the combination of previous reports and our present findings here indicate that while the dissimilar kinetics of the glutamate receptors ($mGluR_6$, AMPA, Kainate) at the photoreceptor-to-bipolar cell synapse[16,17] may initiate the transient vs. sustained response dichotomy in the retina, the great variety in RGC response transience is gained elsewhere in the circuitry[18–20] and we think that it is mainly due to inner retinal inhibitory and/or excitatory interactions.

RGC response transience is altered by the Perturbation of inner retinal lateral inhibition

There is mounting evidence showing that inner retinal GABAergic inhibition is one of the key factors to determine RGC response kinetics, including transience.[11,21–26] To see the extent of GABAergic inhibition on response transience, we blocked the inhibition by using the non-specific $GABA_a/GABA_c$ receptor antagonist PTX ($n = 3$ in a concentration of 50 μM; ON RGC N = 327, OFF RGC N = 286) and recorded RGC responses in both control conditions and under the GABA receptor blockade. As expected, this treatment clearly resulted in a great alteration of RGC responses by diminishing certain response components and enhancing others. In particular, the early, brisk phases of light responses were enhanced while later response components were augmented or blocked completely (Figure 2A). Altogether, the GABA

Table 1. Pharmacological effects on RGC response transience

RGC population	PSTHτ mean (s)	PSTHτ change significance	PSTHτ SD (s)	PSTHτ range (s)
control ON cells	0.109	NA	0. 99	0.02–0.598
control OFF cells	0.137	NA	0.109	0.02–0.592
PTX ON cells	0.073	$p = 3.386*10^{-7}$	0.067	0.02–0.522
PTX OFF cells	0.098	$p = 3.734*10^{-2}$	0.111	0.02–0.567
MFA ON cells	0.083	$p = 3.362*10^{-6}$	0.079	0.02–0.52
MFA OFF cells	0.097	$p = 5.518*10^{-5}$	0.097	0.02–0.56

receptor blockade induced a change that made many RGC responses more transient ($p_{ON} = 0.1*10^{-2}$, $p_{OFF} = 0.46*10^{-2}$; Kolmogorov–Smirnov nonparametric test). When a PSTHτ distribution histogram was generated for both ON ($N = 327$) and OFF ($N = 286$) RGC responses, the outcome differed considerably from the distribution recorded under control conditions (Figure 2B). The relative contribution of intermediate responses (0.08–0.2 s) was considerably reduced, whereas transient RGC responses (0.02–0.06 s) appeared more frequent after the treatment. Note, that the relative contribution of sustained responses (>0.2 s) did not change after the GABA receptor blockade. These changes in the distribution were also reflected by the reduced mean values for both ON- and OFF cells (Table 1). The range of ON and OFF responses were 0.02–0.522 and 0.02–0.567 s following GABA receptor blockade, respectively, thus showing no observable difference when compared to ranges attained in control conditions (Table 1).

Next, we quantified the GABA receptor blockade induced response changes for individual cells. In case of the ON RGC responses ($N = 150$) PTX caused a clear decrease of PSTHτ values for most RGCs (Figures 2C–2E; mean control: 0.126 s +/− 0.057 SD; mean PTX: 0.071 s +/− 0.035 SD). For OFF RGC responses ($N = 100$) we observed a similar GABA receptor blockade induced change as the mean of PSTHτ values dropped from 0.122 s +/− 0.055 SD (in control) to 0.107 ± 0.111 SD under the PTX blockade; this change was significant for both ON and OFF RGC responses (Table 1; $p < 0.05$ for both populations, paired t-test). In conclusion, our data provides evidence that GABAergic inhibition significantly shapes RGC response kinetics.

RGC response transience is altered by the perturbation of gap junction mediated lateral excitation

Besides lateral inhibition, many RGCs receive GJ mediated lateral excitation from neighboring RGCs and/or amacrine cells[36–42] that may serve to further shape the transience of RGC signals. In fact, it has recently been reported that the RGC response delay, another response kinetic feature, is effectively fine-tuned by lateral GJ connections.[3] To investigate if response transience is also a subject of GJ mediated signaling, we applied a pharmacological GJ blockade (MFA) and compared the resulting response kinetics to those recorded under control conditions. The effects of MFA on RGC response transience were initially examined using three different drug concentrations, 20, 40 and 80 μM of MFA. MFA induced changes in all three experiments, and a clear dose dependent effect was observable when the transience distribution histograms were compared (Figures S1A and S1B). Clearly, the lowest tested concentration of MFA (20 μM) already altered the RGC PSTHτ distributions, and this effect was further enhanced following incubation with 40 μM MFA, with the greatest degree of disturbance recorded when the concentration was further increased to 80 μM. However, 40 μM MFA already produced clear results ($p < 0.05$, Wilcoxon signed rank test) and thus, to reduce the chance of potential nonspecific effects, we utilized this as the final MFA concentration in the rest of the experiments.

As previously noted, we observed a great alteration of RGC responses following the application of MFA (40 μM), which was present for both the ON ($N = 598$) and OFF ($N = 187$) RGC subpopulations (Figures 3A and 3B). Although the effect of the pharmacological blockade varied from cell to cell, an overall decrease in PSTHτ was observed across both the ON and OFF RGC subpopulations ($p_{ON} = 0.16*10^{-1}$, $p_{OFF} = 0.13*10^{-1}$; Kolmogorov–Smirnov nonparametric test) and these changes appeared significant (Table 1; $p < 0.05$ for both populations; Wilcoxon signed ranks test). Therefore, akin to effects of GABA receptor inhibition, the GJ pharmacological blockage made the overall RGC responses somewhat more transient. To confirm these latter pharmacological data we repeated the experiments (retinas $n = 3$, ON $N = 266$, OFF $N = 271$ cells) by using the Cx36/Cx50 specific quinine (100 μM;[43–45]) to block retinal GJs. The effects of quinine on RGC light responses were very similar to those of the MFA results (Figures 3F; S1B, S1C, and S1D), including a similar PSTHτ frequency histogram ($pON = 0.26*10^{-9}$, $pOFF = 0.128*10^{-3}$; Kolmogorov–Smirnov nonparametric test) as well as a great variety in PSTHτ changes of individual RGC responses. This thus further confirmed that signaling through GJs can alter response kinetics like transience non-uniformly. Finally, we also utilized constitutive connexin36 knock-out (Cx36KO) to verify the previous pharmacological GJ blockade data. We found that the PSTHτ frequency histograms generated upon light responses of Cx36KO RGCs (retinas $n = 4$, ON $N = 64$, OFF $N = 75$ cells) displayed a similar shape to those of the MFA treated RGCs (Figure S1E). Although, we admit that the above constitutive Cx36 KO data does not clarify the specific site of drug action obtained in the pharmacological experiments, but the similar results gained by two different approaches support our hypothesis that signaling via Cx36 GJ greatly determine RGC response kinetics including transience.

However, despite the similar frequency distributions of the control data to those where GJ connections were compromised (either MFA or quinine blockade, as well as the Cx36 KO) individual RGC responses were greatly affected; the GJ closure induced an RGC transience reduction for a subset of the cells, whereas another population of RGC responses endured a transience increment (Figures 3C–3E; Figure S1). To quantify the magnitude of GJ blockade induced changes to those that were exerted by the GABA receptor blockade we compared
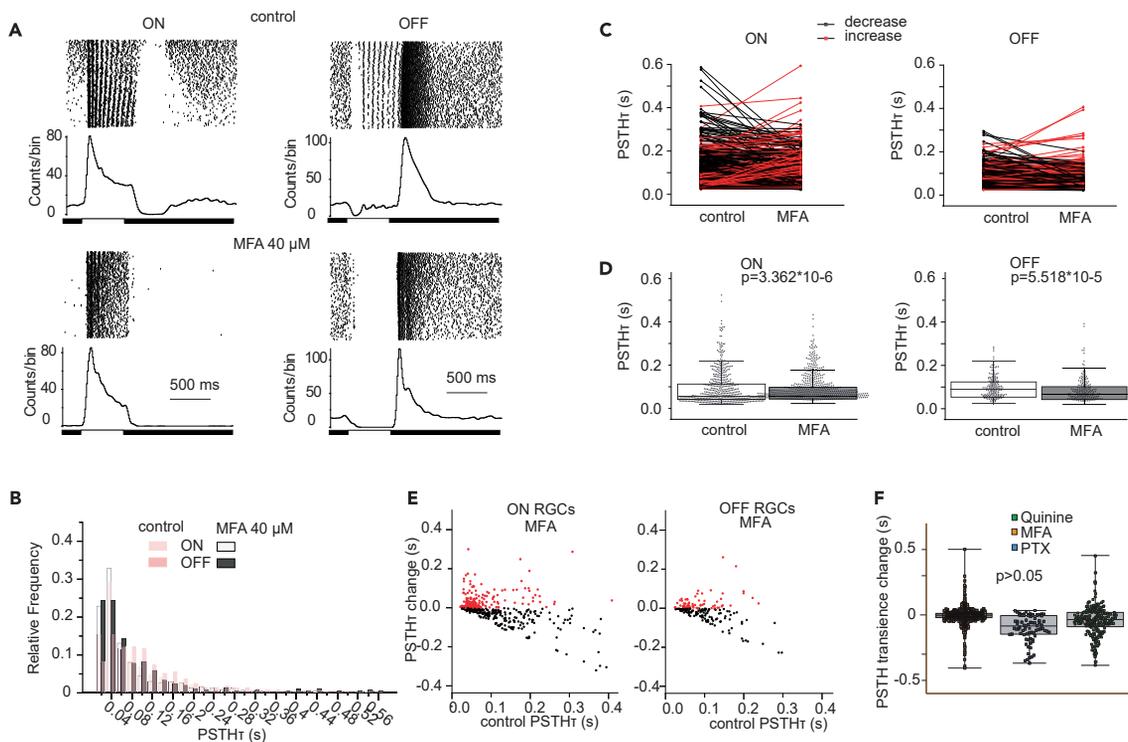
Figure 3. Pharmacological GJ blockade induces alterations in RGC response transience

(A) Representative ON (left) and OFF (right) RGC light-evoked responses (rasters on the top and PSTHs on the bottom) are altered when the nonspecific GJ blocker was MFA applied. In the case of the two presented RGC responses, the ON center cell (left) maintained the same response characteristics (remains intermediate), whereas the OFF RGC response (right) changes from intermediate to transient following MFA treatment.

(B) Frequency histograms show that the elimination of GJ communication somewhat decreased the number of RGCs with intermediary responses, whereas the relative frequency of transient RGC responses became greater.

(C–E) While some RGCs showed no obvious change in their PSTH$_\tau$ values following the GJ blockade, most RGC responses became either more transient or more sustained (C) for both the ON- (left) and OFF subpopulations (right). Although, MFA mediated a significant transience decrease of the averaged data for both ON (left) and OFF (right) RGC subpopulations ($p < 0.05$, Wilcoxon signed rank test) (D), the magnitude of the drug induced change was not evident due to the heterogeneous cell-to-cell changes (C, E). Like the GABAergic blockade, many sustained RGC responses became more transient following the GJ blockade. In addition, however, many transient RGC responses became more sustained as well (C, E; positive dimension reflects a transient-to-sustained, whereas negative dimension reflects a sustained-to-transient change).

(F) The comparison of the PTX and MFA data show that the GJ blockade alters transience values as much as the pharmacological GABAergic blockade, however, while PTX mostly lowers transience values (light blue), MFA alters them in both directions (orange) ($p < 0.05$, Wilcoxon signed rank test). Note, that a similar pharmacological treatment with the Cx36/Cx50 selective quinine exerted a change of the RGC responses (green) similar to those of the MFA effects (see also Figure S1). Shown are mean values (line), 25% and 75% quartiles (boxes), standard deviation (whiskers).

the PSTH$_\tau$ value changes (PSTH$_\tau$ after blockade - PSTH$_\tau$ in control) collected in the PTX experiments with those of the MFA experiments. We found that response transience changes induced by the two pharmacological interventions were significantly different ($p > 0.05$); while PTX induced a general PSTH$_\tau$ reduction, the application of MFA exerted either an increase or a decrease of RGC response transience values. Similarly, quinine induced a change of RGC PSTH$_\tau$ values, which was significantly different from changes caused by the PTX induced GABA receptor blockade ($p > 0.05$). Thus, our comparison reinforced the above qualitative finding (Figure 3F) and strongly suggested the GJ mediated excitatory signals exert diverse effects in shaping RGC response kinetics.

GJ connections shape response transience of electrically coupled RGCs heterogeneously

The mammalian retina incorporates various types of GJ connections that exert a mixture of effects on RGC response transience. However, selective GJ blockers to target specific GJ circuit elements are not currently available. On the other hand, it has been well established that RGC-RGC and RGC-amacrine cell GJs serve the correlation of RGC spiking activity, providing specific bimodal and/or unimodal peaks in cross-correlation functions (CCFs) generated upon RGC pair recordings, respectively.[17,42,46–50] This allowed us to use the presence of CCF peaks to identify and separate RGCs that maintain such GJ connections from those that either lack these connections or are being recorded without the coupled neighbors. Our hypothesis was that RGCs maintaining similar GJ connections (RGC-RGC or RGC-AC) should endure similar changes (uniform decrease or increase) of the response transience following the GJ blockade across the subpopulation. To test this hypothesis, we recorded RGC spike responses ($N = 1344$) evoked by full-field stimuli with a multielectrode array (4096 HD-MEA) under
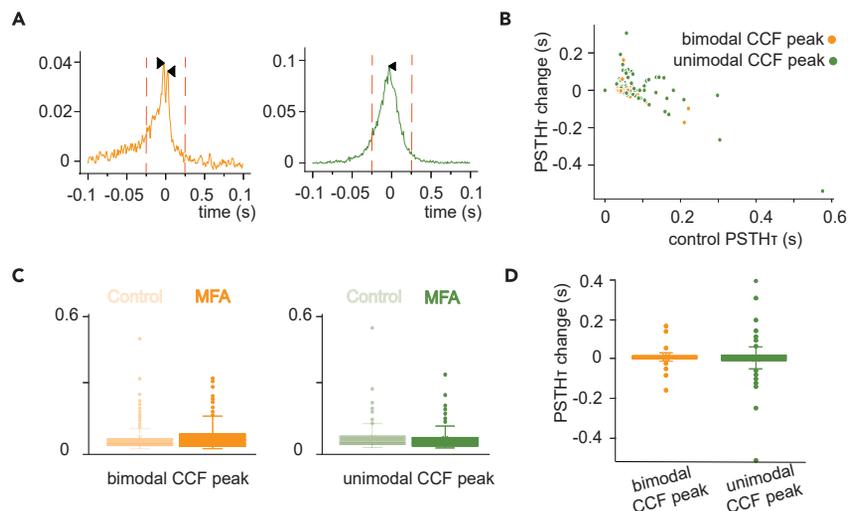
Figure 4. The pharmacological GJ blockade exerts a heterogeneous effect on the response transience of electrically coupled RGCs

(A) RGC CCFs display bimodal (left) or narrow unimodal (right) spikes correlations generated upon RGC pair recordings. Arrowheads point to CCF peaks, whereas dashed lines at +/− 25 ms attest the short timescale of both CCF peak types.

(B) Scatterplot shows MFA induced transience changes (positive dimension reflects a transient-to-sustained, whereas negative dimension reflects a sustained-to-transient change) as a function of original transience values for the two cell populations (orange – cells with bimodal CCF peaks; green – cells with narrow unimodal CCF peak). It appears that both populations contain cells that endured significant transience change as a response to MFA incubation.

(C) Boxplots summarize the effects of the pharmacological GJ blockade of the population of RGCs with bimodal CCF peaks (left) and narrow unimodal peaks (right; note that absolute values are shown to focus on the magnitude of the change). Clearly, the heterogeneous MFA induced RGC response transience changes resulted in little alteration of the averaged data.

(D) Box-plot shows the variety of MFA induced transience changes for both RGC populations. Following MFA treatment only a few RGCs showed no significant transience change, whereas most endured either a decrease or an increase of their PSTHτ values. Shown are mean values (line) , 25% and 75% quartiles (boxes), standard deviation (whiskers)

both control conditions and following the pharmacological blockade of GJs (MFA 40 μM). Using the CCF based criterion, we sorted the recorded RGCs, and those displaying either bimodal or narrow unimodal CCF peaks were used for further analysis. We found that the pharmacological GJ blockade induced the alteration of response transience for cells in both the uni- and bimodal peak subpopulations (Figure 4; unimodal PSTHτ change mean:0.007), bimodal PSTHτ change mean: 0.001). Surprisingly, the GJ blockade induced changes were still heterogeneous; while some RGC responses became more transient others appeared more sustained following the pharmacological intervention. This change was independent of the subpopulation as some cell response transience decreased while others increased in both the uni- and bimodal peak cell groups. This observation serves as further evidence that inner retinal RGC GJ connections partake in response transience fine-tuning. On the other hand, the effect of the pharmacological blockade was still heterogeneous regardless of the selective investigation of GJ coupled RGCs indicating that the observed changes were independent of the GJ connection type (RGC-RGC or RGC-AC).

RGC gap junctions participate in the response transience fine-tuning of transient OFF alpha cells

The above shown heterogeneous effects of the GJ blockade suggested that light responses were indeed shaped by various underlying mechanisms in an RGC subtype specific fashion. As a result, we focused our investigations on a single RGC subtype, the transient OFF alpha (tOFFα) RGC (Figure 5). We recorded from RGCs (N = 12) of Thy1-GCamP3 mice with a PC pipette, and the intracellular solution contained either MFA (40 μM) or the Cx36/Cx50 specific quinine (100 μM;[43–45]). By using this recording configuration, we avoided the blockade of outer retinal GJs and focused our pharmacology on blocking only the GJ connections of the recorded RGC. This way the pharmacological treatment retains the function of outer retinal and other inner retinal GJ network elements. The identity of recorded tOFFα cells was confirmed by the injection of Neurobiotin and corresponding post-hoc histology (Figure 5A). The tOFFα RGC processes included in the experiment displayed standard characteristic features including a large soma, sparse dendrites, and dendritic endings in the OFF sublamina.[39,41,51] Furthermore, the co-stratification of RGC dendritic endings with HCN4 (hyperpolarization-activated cyclic nucleotide-gated channel 4) positive type 3a bipolar cell axon terminals also confirmed the identity of our tOFFα RGCs (Figure 5A;[52]). In addition to the morphological cues, targeted cells were also tested for their light evoked activity. RGC spike trains were recorded in a loose-patch configuration from visually targeted tOFFα RGCs in the Thy1-GCamP3 mice. We utilized large (500 μm in diameter) bright and dark spots to determine the response polarity of the targeted cell. We also utilized a small dark spot stimulus with gradually increasing diameter (from 40 μm to 240 μm; approach stimulus) as well as a moving dark bar stimulus (400 μm/s). In definition, tOFFα RGCs are OFF polarity cells and can differentiate between the approach and the lateral motion. Therefore, we only utilized data for further analyses that we obtained from cells that fulfilled both the morphological and the electrophysiological criteria. Following the unequivocal identification, full-field stimulus evoked spike trains were recorded in a
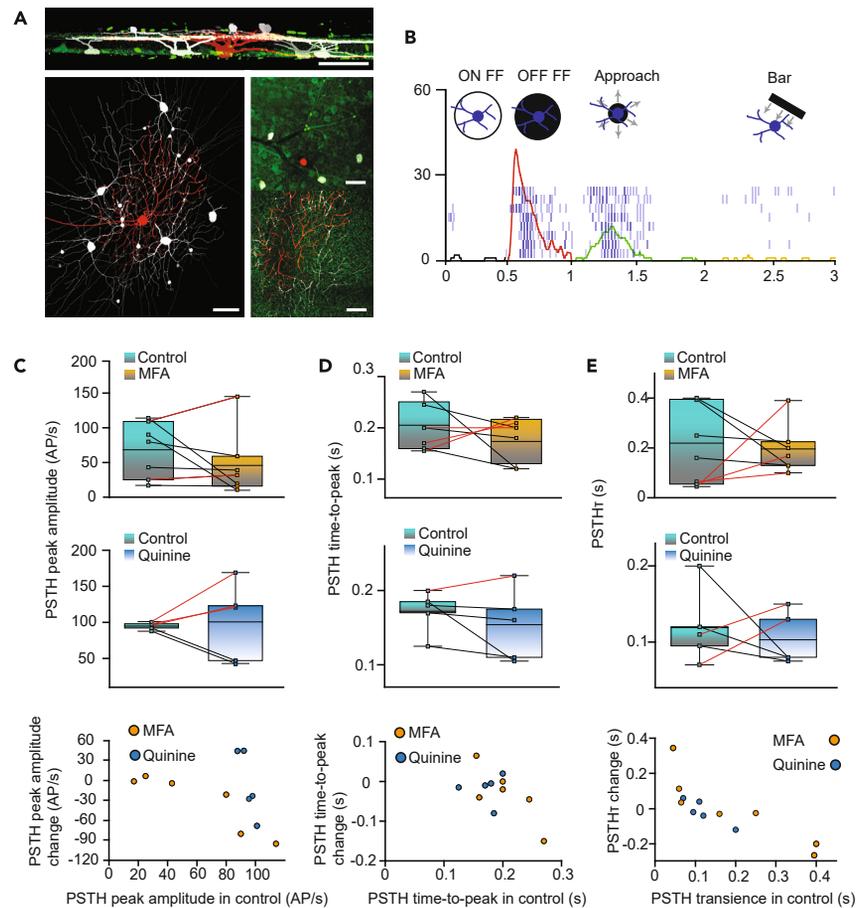
Figure 5. Identification of tOFFα cells and effects of RGC GJs in response kinetics

(A) Images show the Neurobiotin coupled array of an injected tOFFα RGC (red). Besides the injected cell Neurobiotin revealed the soma/dendritic morphologies of both the GJ coupled neighbor RGCs (large white somata and dendrites) and wide-field amacrine cells (small white somata and dendrites). The panel on the top shows the same Neurobiotin coupled array rotated with 90° to reveal the dendritic stratification of both the injected and the tracer coupled cells. The green counterstaining represents the a-HCN label that marks the stratification of type 3a bipolar cell axonal terminals in the IPL. Injected and coupled cell dendrites clearly colocalize with type 3a bipolar cell dendrites. Panels to the right show the same coupled array at the level of the RGC somata (top panel; red – injected, white – coupled) as well as in the IPL (bottom panel) where HCN4 positive type 3a bipolar cell axons stratify (green). Note, that the injections were performed in the Thy1-GCamp3 mouse retina and some green labels of RGC somata appear in the GCL.

(B) Spike recordings of a representative tOFFα RGC (PSTHs overlaid the corresponding spike rasters). Pictograms on the top represent the light stimuli utilized to evoke the responses below. The stimuli included large bright spot (full-field illumination), large dark spot, approach stimulus (spot with increasing diameter) and lateral moving dark bar.

(C) Targeted tOFFα RGC full-field spiking responses were recorded in a loose-patch configuration. tOFFα RGCs response amplitudes displayed heterogeneous changes as a result of the GJ blockade by either MFA (top) or quinine (bottom). Drug-induced response amplitude changes varied considerably from cell-to-cell (decreased: $N = 6$, increased: $N = 2$ and remained constant: $N = 3$).

(D) Response delay (time-to-peak) values of coupled tOFFα RGCs display heterogeneous changes as a result of the GJ blockade by either MFA (top) or quinine (bottom). We found that both drugs induced transience changes that varied considerably from cell-to-cell (decreased: $N = 5$, increased: $N = 2$ and remained largely constant: $N = 4$).

(E) Response transience values of tOFFα RGCs displayed heterogeneous changes as a result of the GJ blockade by either MFA (top) or quinine (bottom). We found that both drugs induced transience changes that varied considerably from cell-to-cell (decreased: $N = 6$, increased: $N = 5$ and remained largely constant: $N = 1$). Clearly, kinetic features of visually targeted tOFFα RGCs endured an abrupt but heterogeneous change as a result of the pharmacological GJ blockade. Scale bar: 50 μm. Shown are mean values (line), 25% and 75% quartiles (boxes), standard deviation (whiskers).

loose-patch configuration from targeted tOFFα RGCs in Thy1-GCamP3 mice ($n = 12$; Figure 5C) under both control conditions and GJ blockade. We found that the application of either MFA or quinine induced abrupt changes of the tOFFα RGCs light responses. These changes affected all three response kinetic features, including the amplitude, transience, and delay values of RGC responses. Interestingly, however, the changes exerted by either MFA or quinine application were rather heterogeneous. More specifically, some targeted tOFFα RGCs response amplitudes decreased ($N = 6$) while others increased ($N = 2$) or showed no considerable alteration ($N = 3$). A similar GJ blockade induced variety of tOFFα RGCs response delay (time-to-peak) values were also detected; some cells displayed a GJ blockade induced delay
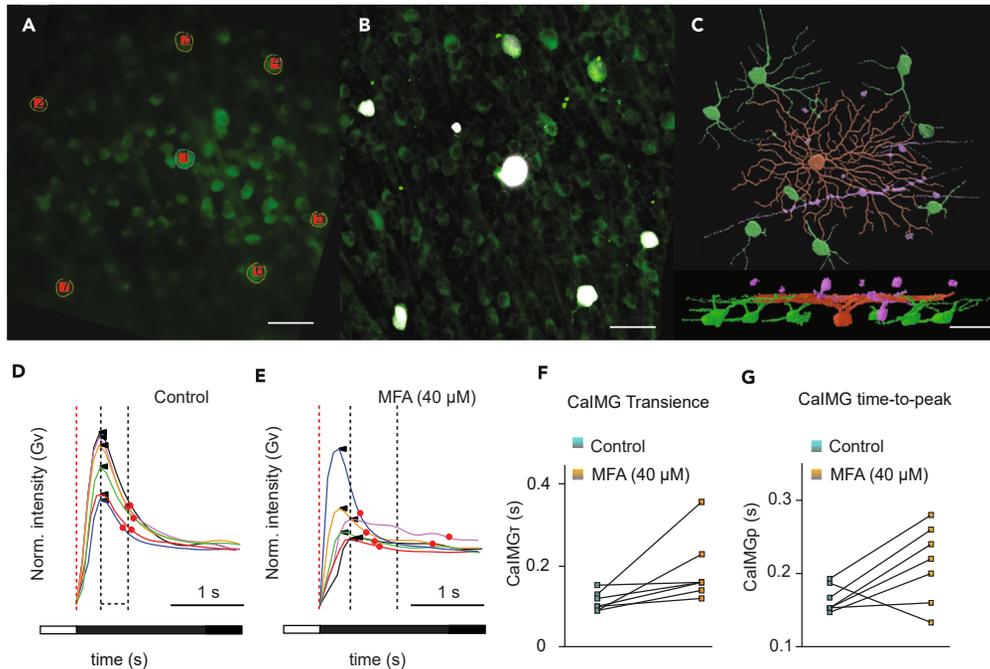
Figure 6. tOFFα cells of the coupled array display heterogeneous response kinetic changes following GJ closure

(A) Panels show RGC somata (red) on the surface of the Thy1-GCamp3 retina.

(B and C) Panels show the somata (B) and the dendritic morphology (C) of the NB injected (red) and tracer coupled RGCs (green) and coupled amacrine cells (purple). Both the injected cell and the NB coupled RGC neighbors displayed dendritic morphological characteristics of tOFFα cells.

(D and E) Light evoked Ca^{++}-transients of injected (black trace) and tracer coupled tOFFα RGCs (colored traces) display similar response kinetics in control measurements, including the delay and the transience (D). Arrowheads point to the peaks of the recorded RGC Ca^{++}-transients, red dots mark PSTHτ values for each wave and the white and black areas of the bar below the recordings show the on- and offsets of the light stimuli. Clearly, both the response onsets and the decay time (slope) are comparable for all recorded cells in this array. However, following a pharmacological GJ blockade (E) both response delay and transience values endured changes that varied from cell-to-cell, as represented by the irregular timing of wave peaks (black arrow) and PSTHτ values (red dots).

(F and G) Delay (F) and transience (G) values of individual RGCs of the array (same as in panels A–E) are shown in control (light blue) and GJ blocked (orange) conditions. RGCs of this coupled array endured significant response kinetic alterations following the GJ blockade. In this array the application of MFA induced an increase of the transience ($N = 5$) or no change ($N = 1$) as well as a decrease ($N = 1$), an increase ($N = 5$) or no change ($N = 1$) for the response delay values (see also Figure 7 for more data). Scale bar: 50 μm.

decrease ($N = 5$), others showed a delay increase ($N = 2$) whereas a third cohort showed no considerable delay change ($N = 4$). Finally, the response transience values decreased for some ($N = 6$) cells, while others showed an increase ($N = 5$) or no considerable change ($N = 1$) as a result of the GJ blockade. Clearly, kinetic features of visually targeted tOFFα RGCs endured an abrupt but largely heterogeneous change following the closure of GJs, thereby arguing against the RGC subtype specific GJ mediated response kinetic tuning.

Gap junctions equalize response kinetics of electrically coupled transient OFF alpha cells

That said the heterogeneous effects of the GJ blockade on tOFFα response transience were initially surprising as we expected RGCs of the same subtype to behave similarly under uniform conditions. To examine this further, we decided to record responses of tOFFα cell neighbors that formed the same GJ coupled array, with the belief that GJs contribute similarly to the response transience for tOFFα cells that are in direct GJ contact with one another. To this end, we chose Ca^{++}-imaging that allowed us to morphologically identify both the recorded tOFFα cells as well as the GJ coupled neighbors. We carried out Ca^{++}-imaging tests in Thy1-GCamP3 mice ($n = 8$), where tOFFα RGCs were targeted based on the size and shape of their soma (Figure 6A). We also combined the Ca^{++}-imaging tests with intracellular Neurobiotin tracer injections and *post hoc* histology. The tracer injections allowed for the *post hoc* identification and the examination of the Ca^{++}-transients of the tracer coupled RGCs as well. Similar to the previous set of experiments, the dendritic morphology and the dendritic co-stratification with a-HCN4 labeled bipolar cell axon terminals were utilized as a guidance for tOFFα cells identification (Figure 6B). Besides the morphological features, the light induced Ca^{++}-transients of both injected and coupled tOFFα RGCs displayed OFF polarity responses that supported the tOFFα identity further (Figures 6C and 6D). In these experiments, light induced Ca^{++}-transients of identified tOFFα RGCs and Neurobiotin coupled RGCs neighbors were examined under control conditions and following MFA (40 μM) incubation. We found that the light response kinetics of the GJ coupled array forming tOFFα RGCs were rather homogeneous in control conditions, but the kinetic parameters (delay, transience, amplitude) were clearly altered by the GJ blockade (Figures 6D and 6E). Interestingly, however, this alteration was still
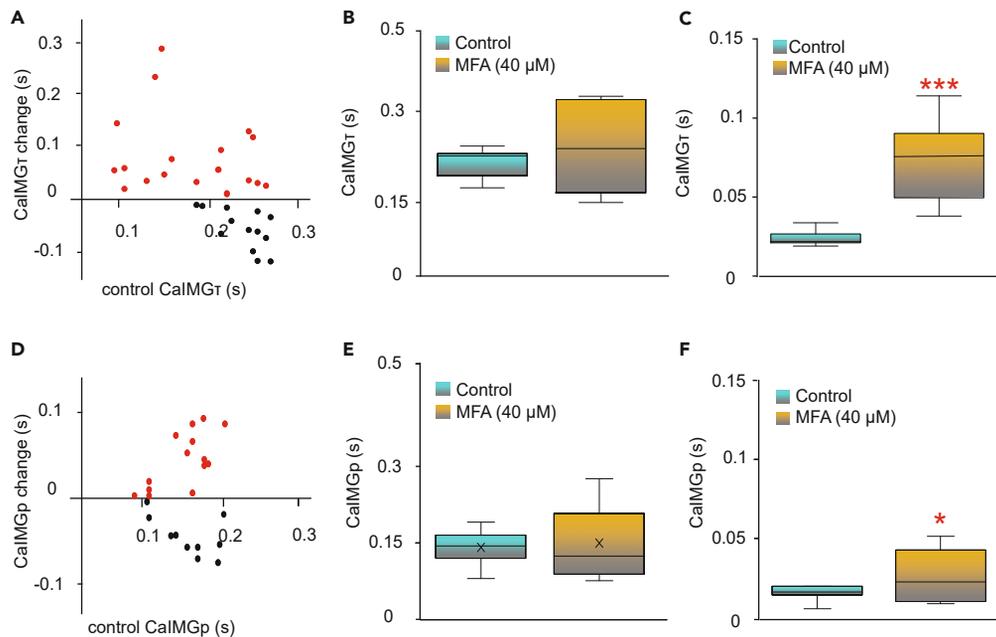
Figure 7. Ca^{++}-signal Kinetics are Equalized by the RGC GJ Connections

(A and D) Scatterplots (A and D) showed pooled data from $n = 8$ tOFFα arrays. Both delay (A) and transience (D) values changed in a rather heterogeneous fashion, with most RGCs either increasing or decreasing delay and transience values.

(B–F) Boxplots show the average (B, E) and the SD values (C, F) of control (green) and MFA (yellow) treated RGC responses for response transience (B, C) and delay (E, F). Although the GJ blockade exerts no significant change of the average delay and transience values, their range and the SD values significantly increased as a result of MFA treatment (transience: ***$p < 0.001$, Wilcoxon signed rank test, panel c; delay: *$p < 0.05$, Wilcoxon signed rank test, panel F). Shown are mean values (line), 25% and 75% quartiles (boxes), standard deviation (whiskers).

heterogeneous. Response transience values of some tOFFα RGCs in the array decreased or remained unaltered, while increased for others following the pharmacological treatment (Figures 6D–6F and 7A). Similarly, the pharmacological GJ closure induced a response delay (time-to-peak) reduction for some cells in the array while an increment could be observed for others (Figures 6D, 6E, 6G, and 7D).

These results indicate that contrary to our expectations GJ connections do not simply shift response kinetics to a specific direction for cells in the coupled array, but rather serve as kinetic feature equalizers. By this equalization mechanism, tOFFα cells in a particular GJ coupled array can send signals toward the brain with very similar kinetics. To see how general this finding was among coupled tOFFα RGCs, we pooled data from $n = 8$ arrays for further analysis (Figure 7). We found that the GJ closure induced heterogeneous response kinetic change was a general phenomenon. In fact, the GJ blockade induced an increased range of both response transience (Figures 7A and 7B) and delay values (Figures 7D and 7E), both of which were confirmed by the significantly increased SD values (transience: $p < 0.001$, Wilcoxon signed rank test, Figure 7C; delay: $p < 0.05$, Wilcoxon signed rank test; Figure 7F).

DISCUSSION

Methodological considerations

The present study is based on a combination of imaging, electrophysiological and pharmacological experiments carried out on wild-type (WT) as well as Cx36 KO mice. Note, neither our pharmacological experiments nor the utilization of constitutive Cx36 KO mice specifically targets RGC GJs due to the non-specificity of the applied drugs as well as the abundancy of the Cx36 subunit in diverse retinal connections. In the KO animal the genetical deletion of Cx36 results a permanent change in the retinal circuitry and may even affect its development, whereas our GJ blockage pharmacology was carried out on WT animals and the functioning of the circuit was only altered temporally. Moreover, while the same tissues (and therefore the same recorded neurons) serve as controls in the pharmacological experiments, tissues from WT littermates provide control measurements in the genetical approach. Therefore, contrary to the same goal the genetical and pharmacological approaches of this study are very different in terms of their modalities. To refine our pharmacological approach, we applied quinine in some experiments, which compound is specific to Cx36 and Cx50 GJ subunits,[44] thereby narrowing down the number of possible targets of GJ silencing pharmacology. This latter fact explains why MFA was, in general, somewhat more effective than quinine. However, contrary to the above differences in the genetical and the two pharmacological approaches the obtained results were rather similar. This thus indicates the observed changes in the measured kinetic parameters, in fact, occurred on Cx36 GJ sites while other GJs were involved to a lesser extent.

That said, one of the key experiments of this study was the targeted electrophysiological recording from tOFFα cells while GJs of the recorded cell were pharmacologically closed by MFA or quinine. This experiment assumes that the applied GJ blockers penetrate through the

cell without binding to extracellular domains and thus affecting Cx subunits only from the intracellular side. The available literature is inconsistent regarding the efficiency of such an approach. Some of the corresponding descriptions report that fenamates (like MFA) do not act on GJs from the intracellular side.[53–55] However, these reports differ from our investigations in the following respects: (1) Pan et al.[53] report the effect of GJ blockers in horizontal cells and AII amacrine cells, not RGCs like in this study; (2) They examine dye and tracer transfer and do not include physiology[53]; thus any discrepancy between that study and our present work can be explained with different intracellular diffusion of charge carrying ions and relative large tracer molecules; (3) Pan et al. applied GJ blockers through high resistance (R > 100 MΩ resistance) sharp electrodes while the experiments of our study were carried out with low-resistance patch electrodes allowing for a better diffusion of the drug into the cytoplasm; (4) Harks et al.[54] examined rat kidney fibroblast in *in vitro* expressional systems not neurons; (5) In Harks' study Cx43 was tested not Cx36, moreover the Cx43 protein was overexpressed which may cause reduced effect of the pharmacological GJ blockade; and (6) Srinivas and Spray[55] utilized neuroblastoma cell cultures, again, not retinal tissue like in our study – they tested cells that express Cx50, Cx26, and many others but not Cx36, and only flufenamic acid (FFA) was applied through the recording pipette. On the other hand, the same authors in one of their other studies[55] found that administration of quinine successfully blocked GJs from the intracellular side. In fact, we utilized both quinine and MFA in our pipette-loaded pharmacology experiments and observed similar effects indicating similar blocking mechanisms of the two drugs. Knowing that quinine is specific to Cx36 and Cx50 gap junctions[55] we believe that we were able to block Cx36 GJ from the intracellular side in tOFFα cells just like it was reported in the 2001 Srinivas study.

Inner retinal GJs participate in the fine-tuning of RGC response transience

The transient/sustained division of RGC light responses has widely been utilized to characterize and classify RGC subtypes, and this characteristic is thought to be strongly related to visual function. In that sense, transient (burst-like) responses likely transmit information about 'fast-paced' and dynamic aspects of the visual field, including direction and movement, whereas sustained responses provide a continuous feed of information on static aspects of the view.[1–3] For example, midget RGCs of the primate retina provide a tonic response to high contrast stimuli, while primate parasol cells have phasic responses to spatially extended stimuli with very weak contrast.[4,56] Therefore, transient and sustained RGC responses encode dissimilar but equally important facets of visual information. This transient/sustained dichotomy has been documented in various vertebrates including cold-blooded animals, primates and non-primate mammals.[4–11,13,14,57] However, the most elaborate studies in this topic were restricted to only a few RGC subtypes,[57] most of which examined the non-image-forming melanopsin expressing ipRGCs. In addition, they were conducted in cold-blooded vertebrates[16] and/or carried out in retinal slice preparations[16,17] where lateral connections were compromised. Previous reports from other labs as well as our previous work[18,19] show that regardless of the analyzing method, RGC light responses cannot be unequivocally divided into clear transient or sustained categories. Instead, RGC PSTHτ-s, values that quantify response transience, fell over a broadly distributed continuous range. These earlier observations were reinforced here showing that the decay of RGC full-field light responses ranged from 0.02 s up to 0.5 s under maintained 0.5 s illumination, and the majority of the cells displayed intermediate values in the 0.07–0.25 s subrange for both the ON and OFF subpopulations. This thus affirms that the canonical transient/sustained categorization is a rather coarse way of RGC response characterization, as many RGCs fail to match the defining characteristics of either transient or sustained RGC light responses. For that reason, we believe that rather than forcing all RGCs into these two categories responses are better depicted by the single value of the full-field PSTHτ.[18]

We also showed evidence here that vertical signaling elements are not the key factors in determining RGC response transience, including: (1) signaling through the sole primary rod pathway resulted in both transient and sustained RGC responses; (2) scotopic RGC response transience values were distributed across a range as broad as those recorded in photopic conditions; (3) some RGCs maintained response kinetics even during a signaling pathway switch that occurs when photopic stimuli replace scotopic counterparts; and (4) transience is fine-tuned by inner retinal lateral GJ connections. These data thus strongly suggest that RGC transience is not (or not entirely) determined by the vertical signaling route but rather established through lateral connections in the two plexiform layers. One may argue that the outer retinal connections are the key in this process. However, GABAergic horizontal cells in the outer retina provide a uniform inhibition to postsynaptic partners, which does not entirely justify the detected diversity of transience changes following the GABA receptor blockade. The role of GABAergic inhibition in shaping RGC response transience is not surprising, as it has been shown previously by many laboratories.[7,58–67] Moreover, it has been shown that axotomized bipolar cells display a great loss of chloride currents,[68] and RGCs displayed more sustained responses when GABAergic amacrine cells were ablated.[11] These converging evidence thus, together with our recent data suggest that the GABA mediated response transience altering inhibitory action occurs mostly in the inner retina.[68]

To our surprise, the effect of the pharmacological GJ blockade on RGC response transience was as robust as those found following the blockade of GABAergic transmission. Although GJs are incorporated in most retinal microcircuits in the mammalian retina,[40,42] the source of the observed GJ blockade on response transience can be narrowed down to a handful of GJ connections. First, outer retinal GJs (e.g., GJs between horizontal cells and those connecting photoreceptors) are constituents of all intraretinal signaling routes, and thus their disturbance likely results in an overall uniform change for all RGC responses, which is inconsistent with our observations. It has also been shown that the genetic deletion of horizontal cell GJs did not have a dominant role in tuning of RGC responses,[69,70] thus their role in shaping response transience is likely negligible as well. Second, GJs formed by rods and/or cones play important roles in scotopic but not photopic signaling, therefore their closure should not be responsible for the RGC response changes we observed under photopic conditions. Therefore, the above combined evidence suggests that much of the GJ blockade induced response transience change can be accounted for by the closure of inner retinal GJs. The most prevalent inner retinal GJs are those formed by AII amacrine cells that connect AII and ON cone bipolar cell neighbors.[40,42,71] However, they play a major role in the primary rod pathway[40,71] and cone mediated

signaling is less affected by AII GJ signaling, thus the observed GJ blockade mediated transience changes cannot be explained simply by their closure. That said the limitations of our study was that the above GJ sites could not be selectively blocked and thus the role of the secondary rod pathway (rod/cone coupling pathway) and AII GJs in the underlying processes could not entirely be ruled out. However, it is more plausible to posit that RGC-RGC and RGC-amacrine cell GJs in the inner retina contribute to the observed response kinetic fine-tuning for several reasons: (1) RGC-RGC and RGC-amacrine cell GJ connections display increased conductivity when the retina is adapted to photopic light conditions thus they likely serve photopic visual functions[72]; (2) similar effects were observed by closing all retinal GJs (MFA experiments), closing Cx36/Cx50 GJ (quinine experiments) and eliminating all Cx36 GJ (constitutive KO mouse experiments) indicating that the responsible molecular component is Cx36, which is also the dominant subunit of RGC-RGC and RGC-amacrine cell GJs[73]; (3) in experiments where the blockers were applied through the pipette, only the recorded cell's GJs were closed but the observed changes in RGC response kinetics were similar to the bath loading experiments; (4) the same pharmacological effect was observed when response kinetics of only tOFFα RGCs of a given coupled array were followed; (5) not all RGCs maintain GJ connection thus some cells are expected to retain response transience following the pharmacological intervention; in fact, a small cohort of our RGCs showed no significant response transience change after the GJ blockade; and, finally, (6) most RGC subtypes (16 out of 22 subtypes) display tracer coupling to nearby RGCs and/or amacrine cells[41] thus a GJ blockade should affect response kinetics of most RGCs, exactly what we found. Therefore, the most parsimonious explanation to our observations is that RGCs, whose light responses endured visible change of their response transience, might be those that partake in such GJ coupling. As the RGC coupling patterns vary considerably in terms of the number, morphology, and dendritic stratification,[37–42,73–75] one may expect a great variety of RGC response transience changes following a pharmacological GJ closure. This theorem agrees with findings reported by Reifler et al.[30] showing that coupling between intrinsically photosensitive RGCs (ipRGC) and displaced amacrine cells allows for signaling between cells, thereby affecting the kinetics of the ipRGC photo response. In experiments presented here, we found an additional example by showing that tOFFα cells endured a change in their full-field response transience following GJ closure. This latter change can also be accounted for by the electrically coupled array of RGCs and amacrine cells. Therefore, we believe that this transience tuning mechanism is not unique to the ipRGC network,[16] but it is a rather general phenomenon involving most GJ coupled RGCs. We showed that electrically coupled RGCs (those with CCF peaks in MEA recordings) displayed a variety of response transience changes following the closure of GJs. This variety in the effect of electrically coupled RGCs and amacrine cells cannot be explained by the simple signal pooling from the extended coupled field, because that would result in a rather homogeneous effect on response transience. At first, this finding suggested that GJ coupling has a subtype specific effect on RGC response transience resulting in changes that are maintained within but varied across RGC subtypes. However, our targeted tOFFα RGC tests showed that even the cell specific GJ blockade (drug applied through the recording pipette) resulted in a variety of response transience (and delay) changes of the coupled RGCs. This indicated that GJs affect response transience throughout a mechanism which is independent of the RGC subtype. This thus rather suggested that the effect of RGC GJs (and the blockade as well) on response kinetics depends on the momentary transjunctional signal flow between the coupled neighbors. Our observations clearly showed that, at least in the GJ coupled tOFFα RGC array, response kinetics were homogeneous when GJs were open, whereas displayed a great variety when GJs were pharmacologically closed. Based on these findings, we conclude that inner retinal RGC GJs serve the equalization of response transience (and all kinetic features) for tOFFα cells in the same electrically coupled array. Moreover, we further suggest that GJ coupling serves the same role for other RGC subtypes as well.

The visual function of RGC transience

In general, we conclude that RGCs collect a cohort of excitatory and inhibitory signals by which they sculpt the output spiking pattern to best suit their function prior to sending information to the brain. This output depends on the type of summated signals and their relative timing; the combination of these two factors may result in a variety of RGC response kinetics on a rather wide transient/intermediary/sustained range. According to this hypothesis, RGCs summate excitatory signals from multiple bipolar cell subtypes and GJ coupled cell neighbors (amacrine and/or RGCs) and filter some of the signal out (via amacrine cell-mediated inhibition) to sway the dominance of input components, thereby adapting to a specific visual function. This is in line with previous reports indicating that certain RGC response properties fully emerge only after additional processing by currents in the bipolar cell axon terminal,[76] at synapses with amacrine cells,[68] and by RGCs. Response transience of these RGCs is not simply inherited from presynaptic bipolar cells but rather transformed by inner retinal inhibition and GJ mediated excitation to suit the necessary RGC visual function. We reported previously that RGC light response delays are subtype-specific, and they are precisely fine-tuned by inner retinal microcircuits to achieve a better RGC performance.[3] It has also been proposed that sustained and transient RGC spiking is another way for various RGC subtypes to perform certain visual functions.[4–14,57] In this scheme, sustained RGCs detect spatial contrasts and partake in shape recognition, whereas transient cells perceive the movement of objects.[1] Similar functional segregation of sustained and transient signals has been reported for other sensory mechanisms as well, including the somatosensory and auditory systems[77]: (1) The Meissner and Pacinian corpuscles in the skin respond transiently (rapidly adapting) because they convey detailed information on light touch and thus persistent signaling would be distracting. On the other hand, signals from nociceptors and muscle spindles must be sustained (slowly adapting) to carry on warning to the brain and to maintain the posture, respectively;[78,79] (2) Primary auditory cortex neurons can be sorted into tonic, phasic-tonic and phasic subtypes that have been thought to relate to their functional difference.[80] Besides sensory processing, neurons of various brain areas also share the labor based on their differential spiking kinetics. For example: (1) Norepinephrine expressing neurons in the pons locus coeruleus can spike in either phasic or tonic modes.[81] Their phasic burst activity is evoked by either salient polymodal sensory stimuli or decision- and response-related signals from the prefrontal cortex,[82–85] whereas tonic firing frequency

correlates with the arousal level of the brain during sleep and waking.[85–88] (2) Neurons in the lateral entorhinal cortex bind sensory events and encode various environmental cues by separate phasic and tonic spiking.[89] (3) Midbrain dopamine neurons encode the rewarding aspects of environmental stimuli (reward, reward prediction error, punishment, stress and sex) as well as cognition and motivation in their phasic, intermediate and tonic activities before signaling the striatum and frontal cortex.[90]

In the retina, the functional divergence already starts at the bipolar cells, as sustained type 1 bipolar cells of the mouse retina mediate color vision for the OFF polarity signaling stream, whereas other, more transient cells do not.[91] Responses of the 30–40 different types of mammalian RGCs[92,93] cover a wide range in terms of their response transience, therefore suggesting a large variety of visual tasks they perform. There has been a considerable collection of evidence supporting this view, including RGCs with transient responses that encode object movement[94–97] and the direction of motion,[98–101] whereas others with sustained responses have been proven to perceive luminosity contrast,[102] color contrast[103] or object orientation.[104] While the first cohort of these RGCs require a quick inactivation and corresponding decay of spiking frequency (transient response) in order to quickly recover and keep up with changes in the visual scene, sustained RGCs allow for the summation of inputs over an extended time frame to get more sensitized for minuscule differences of light levels (e.g., grayscale or color) within their receptive fields. To follow up on this logic one may speculate that the numerous intermediate cells described in this study may serve to encode other parametric dimensions of the visual scene (e.g., wavelength, orientation and/or direction preference, lack of contrast etc.). Alternatively, intermediate cells may convey both spatial and temporal information thereby multiplexing two or more visual features in their spike train. Signal multiplexing by RGCs was first hypothesized by Brivanlou et al.[49] over 20 years ago and this phenomenon is still in the focus of scientific debates. Therefore, the above evidence suggests that the precise adjustment of RGC response temporal features, including transience, is critical for visual perception. Here we found that the precise adjustment of RGC transience is provided in a great part by inner retinal circuits. In essence, RGC GJ mediated lateral excitation, and lateral inhibition provided by GABAergic amacrine cells play an equally important role in this process. In the case of tOFFα RGCs, we showed that GJ connections with nearby RGCs and/or amacrine cells serve as equalizers that fine-tune responses to provide spike RGC outputs that are homogeneous for their kinetic features. Although mostly full-field stimulation was utilized in this study, a complex stimulus dependence of kinetic features is still very likely. It has been reported that the adequate stimulus for tOFFα cells is an increasing dark spot (approach stimulus) and also that faster approach stimuli evoke shorter and higher frequency tOFFα RGC responses, thereby encoding the speed of the stimulus.[94] Since detecting approaching objects, initiating escape behavior, and informing the brain about corresponding changes in the visual field are the primary functions of tOFFα cells, it is very likely that the presented response equalization is a key component for this function. Although the underlying circuit mechanisms yet remain unknown, we formulated a hypothesis based on our present findings. We propose that without such equalization of the response latency and transience, a putative postsynaptic integrator neuron (e.g., in the superior colliculus) may confuse the sequence and the duration of activation of presynaptic units, the electrically coupled tOFFα RGCs. Similarly, the lack of response amplitude equalization may result in the loss of information regarding the extent and/or surface homogeneity of the stimulus. Both defects may hinder the detection of the approaching object and the corresponding decision for the subsequent behavioral pattern (freezing or escaping). Although we did not target other RGC subtypes in this study, it is possible that RGC electrical coupling, in general, serves as a form of response kinetic equalizer for most coupled arrays.

Limitations of the study

One limitation of this study is that neither our pharmacological experiments nor the utilization of constitutive Cx36 KO mice specifically targets RGC GJs. This problem is due to the lack of connexin specific commercially available drugs and site-specific Cx36 KO mouse strains. In our future endeavor we plan to cross PV-Cre and Cx36Flx mice to generate a line in which mice lose GJ contacts specifically between PV expressing cells, including our primary target tOFFα RGCs.[94] Using this line will allow the elimination of RGC GJs while other GJs of the retina remain intact. Alternatively, we plan to inject a virus construct carrying the KCNIP2-Cre sequence (VectorBuilder; https://en.vectorbuilder.com/) intraocularly into the eyes of the Ch36Flx mice. This way we will knock down Cx36 expression in a subset of KCNIP2 (potassium channel interacting protein 2) expressing tOFFα RGCs.[105]

STAR★METHODS

Detailed methods are provided in the online version of this paper and include the following:

- KEY RESOURCES TABLE
- RESOURCE AVAILABILITY
  - Lead contact
  - Materials availability
  - Data and code availability
- EXPERIMENTAL MODEL AND SUBJECT DETAILS
- METHOD DETAILS
  - Extracellular electrophysiology
  - Patch clamp recordings, dye injections
  - Light stimulation
  - Data analysis

- ○ Post hoc histochemistry
- ○ Confocal microscopy and image processing
- ○ Injected cell array reconstructions
- QUANTIFICATION AND STATISTICAL ANALYSIS

AUTHOR CONTRIBUTIONS

Conceptualization, B.V. and G.S.; methodology, G.S and A.G.; validation, B.V., G.K., A.F., and G.S.; formal analysis, G.S., A.G., and A.T.; investigation, G.S., A.G., B.M., F.P., and T.K.-Ö.; resources, B.V.; data curation, G.S., T.K.-Ö., B.M., and A.T.; writing—original draft preparation, B.V. and G.S.; writing—review and editing, B.V., G.S., F.P., A.G., A.T., A.F., T.K.-Ö., and G.K.; visualization, G.S., A.F., and B.V.; funding acquisition, B.V. and G.S. All authors contributed to the article and approved the submitted version.

DECLARATION OF INTERESTS

The authors declare that the research was conducted in the absence of any commercial or financial relationships that could be construed as a potential conflict of interest.

REFERENCES

1. Ikeda, H., and Wright, M.J. (1972). Receptive field organization of 'sustained' and 'transient' retinal ganglion cells which subserve different function roles. J. Physiol. *227*, 769–800. https://doi.org/10.1113/jphysiol.1972.sp010058.

2. Gollisch, T., and Meister, M. (2008). Rapid Neural Coding in the Retina with Relative Spike Latencies. Science *319*, 1108–1111. https://doi.org/10.1126/science.1149639.

3. Tengölics, Á.J., Szarka, G., Ganczer, A., Szabó-Meleg, E., Nyitrai, M., Kovács-Öller, T., and Völgyi, B. (2019). Response Latency Tuning by Retinal Circuits Modulates Signal Efficiency. Sci. Rep. *9*, 15110. https://doi.org/10.1038/s41598-019-51756-y.

4. Gouras, P. (1968). Identification of cone mechanisms in monkey ganglion cells. J. Physiol. *199*, 533–547. https://doi.org/10.1113/jphysiol.1968.sp008667.

5. Werblin, F.S., and Dowling, J.E. (1969). Organization of the retina of the mudpuppy, Necturus maculosus. II. Intracellular recording. J. Neurophysiol. *32*, 339–355. https://doi.org/10.1152/jn.1969.32.3.339.

6. Cleland, B.G., Dubin, M.W., and Levick, W.R. (1971). Sustained and transient neurones in the cat's retina and lateral geniculate nucleus. J. Physiol. *217*, 473–496. https://doi.org/10.1113/jphysiol.1971.sp009581.

7. Caldwell, J.H., and Daw, N.W. (1978). New properties of rabbit retinal ganglion cells. J. Physiol. *276*, 257–276. https://doi.org/10.1113/jphysiol.1978.sp012232.

8. Vallerga, S., and Usai, C. (1986). Relation between light responses and dendritic branching in the salamander ganglion cells. Exp. Biol. *45*, 81–90.

9. Bonaventure, N., Wioland, N., and Roussel, G. (1980). Effects of some amino acids (GABA, glycine, taurine) and of their antagonists (picrotoxin, strychnine) on spatial and temporal features of frog retinal ganglion cell responses. Pflugers Arch. *385*, 51–64. https://doi.org/10.1007/BF00583915.

10. Granda, A.M., and Fulbrook, J.E. (1989). Classification of turtle retinal ganglion cells. J. Neurophysiol. *62*, 723–737. https://doi.org/10.1152/jn.1989.62.3.723.

11. Nirenberg, S., and Meister, M. (1997). The Light Response of Retinal Ganglion Cells Is Truncated by a Displaced Amacrine Circuit. Neuron *18*, 637–650. https://doi.org/10.1016/S0896-6273(00)80304-9.

12. Lu, H.D., and Petry, H.M. (2003). Temporal modulation sensitivity of tree shrew retinal ganglion cells. Vis. Neurosci. *20*, 363–372. https://doi.org/10.1017/S0952523803204028.

13. Wong, K.Y., Dunn, F.A., Graham, D.M., and Berson, D.M. (2007). Synaptic influences on rat ganglion-cell photoreceptors. J. Physiol. *582*, 279–296. https://doi.org/10.1113/jphysiol.2007.133751.

14. Jones, I.L., Russell, T.L., Farrow, K., Fiscella, M., Franke, F., Müller, J., Jäckel, D., and Hierlemann, A. (2015). A method for electrophysiological characterization of hamster retinal ganglion cells using a high-density CMOS microelectrode array. Front. Neurosci. *9*, 360. https://doi.org/10.3389/fnins.2015.00360.

15. Schnapf, J.L., Nunn, B.J., Meister, M., and Baylor, D.A. (1990). Visual transduction in cones of the monkey Macaca fascicularis. J. Physiol. *427*, 681–713. https://doi.org/10.1113/jphysiol.1990.sp018193.

16. Awatramani, G.B., and Slaughter, M.M. (2000). Origin of Transient and Sustained Responses in Ganglion Cells of the Retina. J. Neurosci. *20*, 7087–7095. https://doi.org/10.1523/JNEUROSCI.20-18-07087.2000.

17. DeVries, S.H. (1999). Correlated Firing in Rabbit Retinal Ganglion Cells. J. Neurophysiol. *81*, 908–920. https://doi.org/10.1152/jn.1999.81.2.908.

18. Ganczer, A., Balogh, M., Albert, L., Debertin, G., Kovács-Öller, T., and Völgyi, B. (2017). Transiency of retinal ganglion cell action potential responses determined by PSTH time constant. PLoS One 12, e0183436. https://doi.org/10.1371/journal.pone.0183436.

19. Ganczer, A., Szarka, G., Balogh, M., Hoffmann, G., Tengölics, Á.J., Kenyon, G., Kovács-Öller, T., and Völgyi, B. (2022). Transience of the Retinal Output Is Determined by a Great Variety of Circuit Elements. Cells 11, 810. https://doi.org/10.3390/cells11050810.

20. Kovacs-Öller, T., Ivanova, E., Bianchimano, P., and Sagdullaev, B.T. (2020). The pericyte connectome: spatial precision of neurovascular coupling is driven by selective connectivity maps of pericytes and endothelial cells and is disrupted in diabetes. Cell Discov. 6, 39. https://doi.org/10.1038/s41421-020-0180-0.

21. Dong, C.-J., and Hare, W.A. (2003). Temporal Modulation of Scotopic Visual Signals by A17 Amacrine Cells in Mammalian Retina In Vivo. J. Neurophysiol. 89, 2159–2166. https://doi.org/10.1152/jn.01008.2002.

22. Molnar, A., and Werblin, F. (2007). Inhibitory Feedback Shapes Bipolar Cell Responses in the Rabbit Retina. J. Neurophysiol. 98, 3423–3435. https://doi.org/10.1152/jn.00838.2007.

23. Chen, X., Hsueh, H.-A., Greenberg, K., and Werblin, F.S. (2010). Three Forms of Spatial Temporal Feedforward Inhibition Are Common to Different Ganglion Cell Types in Rabbit Retina. J. Neurophysiol. 103, 2618–2632. https://doi.org/10.1152/jn.01109.2009.

24. Lammerding-Köppel, M., Thier, P., and Koehler, W. (1991). Morphology and mosaics of VIP-like immunoreactive neurons in the retina of the rhesus monkey. J. Comp. Neurol. 312, 251–263. https://doi.org/10.1002/cne.903120208.

25. Lee, C.W., Eglen, S.J., and Wong, R.O.L. (2002). Segregation of on and off Retinogeniculate Connectivity Directed by Patterned Spontaneous Activity. J. Neurophysiol. 88, 2311–2321. https://doi.org/10.1152/jn.00372.2002.

26. Cafaro, J., and Rieke, F. (2010). Noise correlations improve response fidelity and stimulus encoding. Nature 468, 964–967. https://doi.org/10.1038/nature09570.

27. Ackert, J.M., Farajian, R., Völgyi, B., and Bloomfield, S.A. (2009). GABA blockade unmasks an OFF response in ON direction selective ganglion cells in the mammalian retina. J. Physiol. 587, 4481–4495. https://doi.org/10.1113/jphysiol.2009.173344.

28. Farajian, R., Pan, F., Akopian, A., Völgyi, B., and Bloomfield, S.A. (2011). Masked excitatory crosstalk between the ON and OFF visual pathways in the mammalian retina: Excitatory crosstalk between ON and OFF pathways. J. Physiol. 589, 4473–4489. https://doi.org/10.1113/jphysiol.2011.213371.

29. Roy, K., Kumar, S., and Bloomfield, S.A. (2017). Gap junctional coupling between retinal amacrine and ganglion cells underlies coherent activity integral to global object perception. Proc. Natl. Acad. Sci. USA 114, E10484–E10493. https://doi.org/10.1073/pnas.1708261114.

30. Reifler, A.N., Chervenak, A.P., Dolikian, M.E., Benenati, B.A., Meyers, B.S., Demertzis, Z.D., Lynch, A.M., Li, B.Y., Wachter, R.D., Abufarha, F.S., et al. (2015). The rat retina has five types of ganglion-cell photoreceptors. Exp. Eye Res. 130, 17–28. https://doi.org/10.1016/j.exer.2014.11.010.

31. Im, M., and Fried, S.I. (2015). Indirect activation elicits strong correlations between light and electrical responses in ON but not OFF retinal ganglion cells. J. Physiol. 593, 3577–3596. https://doi.org/10.1113/JP270606.

32. Deans, M.R., Volgyi, B., Goodenough, D.A., Bloomfield, S.A., and Paul, D.L. (2002). Connexin36 Is Essential for Transmission of Rod-Mediated Visual Signals in the Mammalian Retina. Neuron 36, 703–712. https://doi.org/10.1016/S0896-6273(02)01046-2.

33. Völgyi, B., Deans, M.R., Paul, D.L., and Bloomfield, S.A. (2004). Convergence and Segregation of the Multiple Rod Pathways in Mammalian Retina. J. Neurosci. 24, 11182–11192. https://doi.org/10.1523/JNEUROSCI.3096-04.2004.

34. Pan, F., Toychiev, A., Zhang, Y., Atlasz, T., Ramakrishnan, H., Roy, K., Völgyi, B., Akopian, A., and Bloomfield, S.A. (2016). Inhibitory masking controls the threshold sensitivity of retinal ganglion cells. J. Physiol. 594, 6679–6699. https://doi.org/10.1113/JP272267.

35. Jin, N., Tian, L.-M., Fahrenfort, I., Zhang, Z., Postma, F., Paul, D.L., Massey, S.C., and Ribelayga, C.P. (2022). Genetic elimination of rod/cone coupling reveals the contribution of the secondary rod pathway to the retinal output. Sci. Adv. 8, eabm4491. https://doi.org/10.1126/sciadv.abm4491.

36. Kántor, O., Szarka, G., Benkő, Z., Somogyvári, Z., Pálfi, E., Baksa, G., Rácz, G., Nitschke, R., Debertin, G., and Völgyi, B. (2018). Strategic Positioning of Connexin36 Gap Junctions Across Human Retinal Ganglion Cell Dendritic Arbors. Front. Cell. Neurosci. 12, 409. https://doi.org/10.3389/fncel.2018.00409.

37. Schubert, T., Degen, J., Willecke, K., Hormuzdi, S.G., Monyer, H., and Weiler, R. (2005). Connexin36 mediates gap junctional coupling of alpha-ganglion cells in mouse retina. J. Comp. Neurol. 485, 191–201. https://doi.org/10.1002/cne.20510.

38. Schubert, T., Maxeiner, S., Krüger, O., Willecke, K., and Weiler, R. (2005). Connexin45 mediates gap junctional coupling of bistratified ganglion cells in the mouse retina. J. Comp. Neurol. 490, 29–39. https://doi.org/10.1002/cne.20621.

39. Völgyi, B., Abrams, J., Paul, D.L., and Bloomfield, S.A. (2005). Morphology and tracer coupling pattern of alpha ganglion cells in the mouse retina. J. Comp. Neurol. 492, 66–77. https://doi.org/10.1002/cne.20700.

40. Bloomfield, S.A., and Völgyi, B. (2009). The diverse functional roles and regulation of neuronal gap junctions in the retina. Nat. Rev. Neurosci. 10, 495–506. https://doi.org/10.1038/nrn2636.

41. Völgyi, B., Chheda, S., and Bloomfield, S.A. (2009). Tracer coupling patterns of the ganglion cell subtypes in the mouse retina. J. Comp. Neurol. 512, 664–687. https://doi.org/10.1002/cne.21912.

42. Völgyi, B., Pan, F., Paul, D.L., Wang, J.T., Huberman, A.D., and Bloomfield, S.A. (2013). Gap Junctions Are Essential for Generating the Correlated Spike Activity of Neighboring Retinal Ganglion Cells. PLoS One 8, e69426. https://doi.org/10.1371/journal.pone.0069426.

43. Gajda, Z., Szupera, Z., Blazsó, G., and Szente, M. (2005). Quinine, a Blocker of Neuronal Cx36 Channels, Suppresses Seizure Activity in Rat Neocortex In Vivo. Epilepsia 46, 1581–1591. https://doi.org/10.1111/j.1528-1167.2005.00254.x.

44. Srinivas, M., Hopperstad, M.G., and Spray, D.C. (2001). Quinine blocks specific gap junction channel subtypes. Proc. Natl. Acad. Sci. USA 98, 10942–10947. https://doi.org/10.1073/pnas.191206198.

45. Szarka, G., Balogh, M., Tengölics, Á.J., Ganczer, A., Völgyi, B., and Kovács-Öller, T. (2021). The role of gap junctions in cell death and neuromodulation in the retina. Neural Regen. Res. 16, 1911–1920. https://doi.org/10.4103/1673-5374.308069.

46. Mastronarde, D.N. (1983). Correlated firing of cat retinal ganglion cells. I. Spontaneously active inputs to X- and Y-cells. J. Neurophysiol. 49, 303–324. https://doi.org/10.1152/jn.1983.49.2.303.

47. Mastronarde, D.N. (1983). Correlated firing of cat retinal ganglion cells. II. Responses of X- and Y-cells to single quantal events. J. Neurophysiol. 49, 325–349. https://doi.org/10.1152/jn.1983.49.2.325.

48. Mastronarde, D.N. (1983). Interactions between ganglion cells in cat retina. J. Neurophysiol. 49, 350–365. https://doi.org/10.1152/jn.1983.49.2.350.

49. Brivanlou, I.H., Warland, D.K., and Meister, M. (1998). Mechanisms of Concerted Firing among Retinal Ganglion Cells. Neuron 20, 527–539. https://doi.org/10.1016/S0896-6273(00)80992-7.

50. Hu, E.H., and Bloomfield, S.A. (2003). Gap Junctional Coupling Underlies the Short-Latency Spike Synchrony of Retinal α Ganglion Cells. J. Neurosci. 23, 6768–6777. https://doi.org/10.1523/JNEUROSCI.23-17-06768.2003.

51. Szarka, G., Hoffmann, G., Kovács-Öller, T., and Völgyi, B. (2023). Serotonin is a gap junction-permeable neuronal tracer in the mouse retina. Front. Ophthalmol. 3, 1151024. https://doi.org/10.3389/fopht.2023.1151024.

52. Müller, F., Scholten, A., Ivanova, E., Haverkamp, S., Kremmer, E., and Kaupp, U.B. (2003). HCN channels are expressed differentially in retinal bipolar cells and concentrated at synaptic terminals. Eur. J. Neurosci. 17, 2084–2096. https://doi.org/10.1046/j.1460-9568.2003.02634.x.

53. Pan, F., Mills, S.L., and Massey, S.C. (2007). Screening of gap junction antagonists on dye coupling in the rabbit retina. Vis. Neurosci. 24, 609–618. https://doi.org/10.1017/S0952523807070472.

54. Harks, E.G., de Roos, A.D., Peters, P.H., de Haan, L.H., Brouwer, A., Ypey, D.L., van Zoelen, E.J., and Theuvenet, A.P. (2001). Fenamates: a novel class of reversible gap junction blockers. J. Pharmacol. Exp. Therapeut. 298, 1033–1041.

55. Srinivas, M., and Spray, D.C. (2003). Closure of Gap Junction Channels by Arylaminobenzoates. Mol. Pharmacol. 63, 1389–1397. https://doi.org/10.1124/mol.63.6.1389.

56. Kaplan, E., and Shapley, R.M. (1986). The primate retina contains two types of ganglion cells, with high and low contrast sensitivity. Proc. Natl. Acad. Sci. USA 83, 2755–2757. https://doi.org/10.1073/pnas.83.8.2755.

57. Zhao, X., Reifler, A.N., Schroeder, M.M., Jaeckel, E.R., Chervenak, A.P., and Wong, K.Y. (2017). Mechanisms creating transient and sustained photoresponses in mammalian retinal ganglion cells. J. Gen. Physiol. *149*, 335–353. https://doi.org/10.1085/jgp.201611720.

58. Amthor, F.R., Oyster, C.W., and Takahashi, E.S. (1984). Morphology of on-off direction-selective ganglion cells in the rabbit retina. Brain Res. *298*, 187–190. https://doi.org/10.1016/0006-8993(84)91167-3.

59. Ariel, M., and Daw, N.W. (1982). Pharmacological analysis of directionally sensitive rabbit retinal ganglion cells. J. Physiol. *324*, 161–185. https://doi.org/10.1113/jphysiol.1982.sp014105.

60. Asari, H., and Meister, M. (2012). Divergence of visual channels in the inner retina. Nat. Neurosci. *15*, 1581–1589. https://doi.org/10.1038/nn.3241.

61. Asari, H., and Meister, M. (2014). The Projective Field of Retinal Bipolar Cells and Its Modulation by Visual Context. Neuron *81*, 641–652. https://doi.org/10.1016/j.neuron.2013.11.029.

62. Dacheux, R.F., and Miller, R.F. (1981). An intracellular electrophysiological study of the ontogeny of functional synapses in the rabbit retina. II. Amacrine cells. J. Comp. Neurol. *198*, 327–334. https://doi.org/10.1002/cne.901980210.

63. Maguire, G., Lukasiewicz, P., and Werblin, F. (1989). Amacrine cell interactions underlying the response to change in the tiger salamander retina. J. Neurosci. *9*, 726–735. https://doi.org/10.1523/JNEUROSCI.09-02-00726.1989.

64. Marchiafava, P.L. (1983). An "antagonistic" surround facilitates central responses by retinal ganglion cells. Vis. Res. *23*, 1097–1099. https://doi.org/10.1016/0042-6989(83)90021-4.

65. Masland, R.H. (1988). Amacrine cells. Trends Neurosci. *11*, 405–410. https://doi.org/10.1016/0166-2236(88)90078-1.

66. Nelson, R., and Kolb, H. (1983). Synaptic patterns and response properties of bipolar and ganglion cells in the cat retina. Vis. Res. *23*, 1183–1195. https://doi.org/10.1016/0042-6989(83)90032-9.

67. Werblin, F.S. (1977). Regenerative amacrine cell depolarization and formation of on-off ganglion cell response. J. Physiol. *264*, 767–785. https://doi.org/10.1113/jphysiol.1977.sp011693.

68. Euler, T., and Masland, R.H. (2000). Light-Evoked Responses of Bipolar Cells in a Mammalian Retina. J. Neurophysiol. *83*, 1817–1829. https://doi.org/10.1152/jn.2000.83.4.1817.

69. Dedek, K., Pandarinath, C., Alam, N.M., Wellershaus, K., Schubert, T., Willecke, K., Prusky, G.T., Weiler, R., and Nirenberg, S. (2008). Ganglion Cell Adaptability: Does the Coupling of Horizontal Cells Play a Role? PLoS One *3*, e1714. https://doi.org/10.1371/journal.pone.0001714.

70. Shelley, J., Dedek, K., Schubert, T., Feigenspan, A., Schultz, K., Hombach, S., Willecke, K., and Weiler, R. (2006). Horizontal cell receptive fields are reduced in connexin57-deficient mice. Eur. J. Neurosci. *23*, 3176–3186. https://doi.org/10.1111/j.1460-9568.2006.04848.x.

71. Bloomfield, S.A., and Völgyi, B. (2004). Function and plasticity of homologous coupling between AII amacrine cells. Vis.

Res. *44*, 3297–3306. https://doi.org/10.1016/j.visres.2004.07.012.

72. Hu, E.H., Pan, F., Völgyi, B., and Bloomfield, S.A. (2010). Light increases the gap junctional coupling of retinal ganglion cells: Light increases coupling between retinal ganglion cells. J. Physiol. *588*, 4145–4163. https://doi.org/10.1113/jphysiol.2010.193268.

73. Pan, F., Paul, D.L., Bloomfield, S.A., and Völgyi, B. (2010). Connexin36 is required for gap junctional coupling of most ganglion cell subtypes in the mouse retina. J. Comp. Neurol. *518*, 911–927. https://doi.org/10.1002/cne.22254.

74. Müller, L.P.d.S., Do, M.T.H., Yau, K.W., He, S., and Baldridge, W.H. (2010). Tracer coupling of intrinsically photosensitive retinal ganglion cells to amacrine cells in the mouse retina. J. Comp. Neurol. *518*, 4813–4824. https://doi.org/10.1002/cne.22490.

75. Völgyi, B., Kovács-Öller, T., Atlasz, T., Wilhelm, M., and Gábriel, R. (2013). Gap junctional coupling in the vertebrate retina: Variations on one theme? Prog. Retin. Eye Res. *34*, 1–18. https://doi.org/10.1016/j.preteyeres.2012.12.002.

76. Protti, D.A., Flores-Herr, N., and Von Gersdorff, H. (2000). Light Evokes Ca 2+ Spikes in the Axon Terminal of a Retinal Bipolar Cell. Neuron *25*, 215–227. https://doi.org/10.1016/S0896-6273(00)80884-3.

77. Sachdev, R.N.S., and Catania, K.C. (2002). Receptive Fields and Response Properties of Neurons in the Star-Nosed Mole's Somatosensory Fovea. J. Neurophysiol. *87*, 2602–2611. https://doi.org/10.1152/jn.2002.87.5.2602.

78. E.R. Kandel, J.H. Schwartz, T.M. Jessell, S. Siegelbaum, A.J. Hudspeth, and S. Mack, eds. (2013). Principles of neural science, 5th ed. (McGraw-Hill).

79. Licker, M. (1999). McGraw-Hill 2000 Yearbook of Science & Technology (McGraw-Hill).

80. Chimoto, S., Kitama, T., Qin, L., Sakayori, S., and Sato, Y. (2002). Tonal response patterns of primary auditory cortex neurons in alert cats. Brain Res. *934*, 34–42. https://doi.org/10.1016/S0006-8993(02)02316-8.

81. Devilbiss, D.M., and Waterhouse, B.D. (2011). Phasic and Tonic Patterns of Locus Coeruleus Output Differentially Modulate Sensory Network Function in the Awake Rat. J. Neurophysiol. *105*, 69–87. https://doi.org/10.1152/jn.00445.2010.

82. Aston-Jones, G., and Bloom, F.E. (1981). Norepinephrine-containing locus coeruleus neurons in behaving rats exhibit pronounced responses to non-noxious environmental stimuli. J. Neurosci. *1*, 887–900. https://doi.org/10.1523/JNEUROSCI.01-08-00887.1981.

83. Aston-Jones, G., and Cohen, J.D. (2005). AN INTEGRATIVE THEORY OF LOCUS COERULEUS-NOREPINEPHRINE FUNCTION: Adaptive Gain and Optimal Performance. Annu. Rev. Neurosci. *28*, 403–450. https://doi.org/10.1146/annurev.neuro.28.061604.135709.

84. Aston-Jones, G., and Cohen, J.D. (2005). Adaptive gain and the role of the locus coeruleus–norepinephrine system in optimal performance. J. Comp. Neurol. *493*, 99–110. https://doi.org/10.1002/cne.20723.

85. Berridge, C.W., and Waterhouse, B.D. (2003). The locus coeruleus–noradrenergic system: modulation of behavioral state and state-dependent cognitive processes. Brain

Res. Rev. *42*, 33–84. https://doi.org/10.1016/S0165-0173(03)00143-7.

86. Aston-Jones, G., and Bloom, F.E. (1981). Activity of norepinephrine-containing locus coeruleus neurons in behaving rats anticipates fluctuations in the sleep-waking cycle. J. Neurosci. *1*, 876–886. https://doi.org/10.1523/JNEUROSCI.01-08-00876.1981.

87. Foote, S.L., Aston-Jones, G., and Bloom, F.E. (1980). Impulse activity of locus coeruleus neurons in awake rats and monkeys is a function of sensory stimulation and arousal. Proc. Natl. Acad. Sci. USA *77*, 3033–3037. https://doi.org/10.1073/pnas.77.5.3033.

88. Hobson, J.A., McCarley, R.W., and Wyzinski, P.W. (1975). Sleep Cycle Oscillation: Reciprocal Discharge by Two Brainstem Neuronal Groups. Science *189*, 55–58. https://doi.org/10.1126/science.1094539.

89. Pilkiw, M., Insel, N., Cui, Y., Finney, C., Morrissey, M.D., and Takehara-Nishiuchi, K. (2017). Phasic and tonic neuron ensemble codes for stimulus-environment conjunctions in the lateral entorhinal cortex. Elife *6*, e28611. https://doi.org/10.7554/eLife.28611.

90. Schultz, W. (2001). Book Review: Reward Signaling by Dopamine Neurons. Neuroscientist *7*, 293–302. https://doi.org/10.1177/107385840100700406.

91. Breuninger, T., Puller, C., Haverkamp, S., and Euler, T. (2011). Chromatic Bipolar Cell Pathways in the Mouse Retina. J. Neurosci. *31*, 6504–6517. https://doi.org/10.1523/JNEUROSCI.0616-11.2011.

92. Baden, T., Berens, P., Franke, K., Román Rosón, M., Bethge, M., and Euler, T. (2016). The functional diversity of retinal ganglion cells in the mouse. Nature *529*, 345–350. https://doi.org/10.1038/nature16468.

93. Tran, N.M., Shekhar, K., Whitney, I.E., Jacobi, A., Benhar, I., Hong, G., Yan, W., Adiconis, X., Arnold, M.E., Lee, J.M., et al. (2019). Single-Cell Profiles of Retinal Ganglion Cells Differing in Resilience to Injury Reveal Neuroprotective Genes. Neuron *104*, 1039–1055.e12. https://doi.org/10.1016/j.neuron.2019.11.006.

94. Münch, T.A., da Silveira, R.A., Siegert, S., Viney, T.J., Awatramani, G.B., and Roska, B. (2009). Approach sensitivity in the retina processed by a multifunctional neural circuit. Nat. Neurosci. *12*, 1308–1316. https://doi.org/10.1038/nn.2389.

95. Ölveczky, B.P., Baccus, S.A., and Meister, M. (2003). Segregation of object and background motion in the retina. Nature *423*, 401–408. https://doi.org/10.1038/nature01652.

96. Roska, B., and Werblin, F. (2003). Rapid global shifts in natural scenes block spiking in specific ganglion cell types. Nat. Neurosci. *6*, 600–608. https://doi.org/10.1038/nn1061.

97. Zhang, Q.-X., Zhang, Y., Lu, R.-W., Li, Y.-C., Pittler, S.J., Kraft, T.W., and Yao, X.-C. (2012). Comparative intrinsic optical signal imaging of wild-type and mutant mouse retinas. Opt Express *20*, 7646–7654. https://doi.org/10.1364/OE.20.007646.

98. Barlow, H.B., and Hill, R.M. (1963). Selective Sensitivity to Direction of Movement in Ganglion Cells of the Rabbit Retina. Science *139*, 412–414. https://doi.org/10.1126/science.139.3553.412.

99. Barlow, H.B., and Levick, W.R. (1965). The mechanism of directionally selective units in

rabbit's retina. J. Physiol. *178*, 477–504. https://doi.org/10.1113/jphysiol.1965.sp007638.

100. Fried, S.I., Münch, T.A., and Werblin, F.S. (2005). Directional Selectivity Is Formed at Multiple Levels by Laterally Offset Inhibition in the Rabbit Retina. Neuron *46*, 117–127. https://doi.org/10.1016/j.neuron.2005.02.007.

101. Taylor, W.R., and Vaney, D.I. (2003). New directions in retinal research. Trends Neurosci. *26*, 379–385. https://doi.org/10.1016/S0166-2236(03)00167-X.

102. Johnson, K.P., Zhao, L., and Kerschensteiner, D. (2018). A Pixel-Encoder Retinal Ganglion Cell with Spatially Offset Excitatory and Inhibitory Receptive Fields. Cell Rep. *22*, 1462–1472. https://doi.org/10.1016/j.celrep.2018.01.037.

103. Dacey, D.M., and Lee, B.B. (1994). The "blue-on" opponent pathway in primate retina originates from a distinct bistratified ganglion cell type. Nature *367*, 731–735. https://doi.org/10.1038/367731a0.

104. Nath, A., and Schwartz, G.W. (2017). Electrical synapses convey orientation selectivity in the mouse retina. Nat. Commun. *8*, 2025. https://doi.org/10.1038/s41467-017-01980-9.

105. Wang, F., Li, E., De, L., Wu, Q., and Zhang, Y. (2021). OFF-transient alpha RGCs mediate looming triggered innate defensive response. Curr. Biol. *31*, 2263–2273.e3. https://doi.org/10.1016/j.cub.2021.03.025.

106. Deans, M.R., Gibson, J.R., Sellitto, C., Connors, B.W., and Paul, D.L. (2001). Synchronous Activity of Inhibitory Networks in Neocortex Requires Electrical Synapses Containing Connexin36. Neuron *31*, 477–485. https://doi.org/10.1016/S0896-6273(01)00373-7.

107. Schindelin, J., Arganda-Carreras, I., Frise, E., Kaynig, V., Longair, M., Pietzsch, T., Preibisch, S., Rueden, C., Saalfeld, S., Schmid, B., et al. (2012). Fiji: an open-source platform for biological-image analysis. Nat. Methods *9*, 676–682. https://doi.org/10.1038/nmeth.2019.

108. Hilgen, G., Sorbaro, M., Pirmoradian, S., Muthmann, J.-O., Kepiro, I.E., Ullo, S., Ramirez, C.J., Puente Encinas, A., Maccione, A., Berdondini, L., et al. (2017). Unsupervised Spike Sorting for Large-Scale, High-Density Multielectrode Arrays. Cell Rep. *18*, 2521–2532. https://doi.org/10.1016/j.celrep.2017.02.038.

109. Satopaa, V., Albrecht, J., Irwin, D., and Raghavan, B. (2011). Finding a "Kneedle" in a Haystack: Detecting Knee Points in System Behavior. In 2011 31st International Conference on Distributed Computing Systems Workshops (IEEE), pp. 166–171. https://doi.org/10.1109/ICDCSW.2011.20.

110. Peirce, J., Gray, J.R., Simpson, S., MacAskill, M., Höchenberger, R., Sogo, H., Kastman, E., and Lindeløv, J.K. (2019). PsychoPy2: Experiments in behavior made easy. Behav. Res. *51*, 195–203. https://doi.org/10.3758/s13428-018-01193-y.

111. Pedregosa, F., Varoquaux, G., Gramfort, A., Michel, V., Thirion, B., Grisel, O., Blondel, M., Müller, A., Nothman, J., Louppe, G., et al. (2012). Scikit-learn: Machine Learning in Python. J. Mach. Learn. Res. *12*, 2825–2830. https://doi.org/10.48550/ARXIV.1201.0490.

112. Sargoy, A., Barnes, S., Brecha, N.C., and Pérez De Sevilla Müller, L. (2014). Immunohistochemical and Calcium Imaging Methods in Wholemount Rat Retina. JoVE *51396*, e51396. https://doi.org/10.3791/51396.

113. Jeon, C.-J., Strettoi, E., and Masland, R.H. (1998). The Major Cell Populations of the Mouse Retina. J. Neurosci. *18*, 8936–8946. https://doi.org/10.1523/JNEUROSCI.18-21-08936.1998.

114. Penn, J.S., and Williams, T.P. (1984). A new microspectrophotometric method for measuring absorbance of rat photoreceptors. Vis. Res. *24*, 1673–1676. https://doi.org/10.1016/0042-6989(84)90325-0.

115. Muthmann, J.-O., Amin, H., Sernagor, E., Maccione, A., Panas, D., Berdondini, L., Bhalla, U.S., and Hennig, M.H. (2015). Spike Detection for Large Neural Populations Using High Density Multielectrode Arrays. Front. Neuroinf. *9*, 28. https://doi.org/10.3389/fninf.2015.00028.

116. Arshadi, C., Günther, U., Eddison, M., Harrington, K.I.S., and Ferreira, T.A. (2021). SNT: a unifying toolbox for quantification of neuronal anatomy. Nat. Methods *18*, 374–377. https://doi.org/10.1038/s41592-021-01105-7.

STAR★METHODS

KEY RESOURCES TABLE

REAGENT or RESOURCE	SOURCE	IDENTIFIER
Antibodies		
DyLight™ 405 AffiniPure Goat Anti-Rabbit	Jackson immuno	Cat# 111-475-003; RRID: AB_2338035
Rabbit anti-5-HT	Sigma-Aldrich	Cat# S5545; RRID: AB_477522
Rabbit anti-ChAT	ThermoFisher	Cat# PA5-29653; RRID: AB_2547128
Rabbit anti-HCN4	Alomone Labs	Cat# APC-052; RRID: AB_2039906
Chemicals, peptides, and recombinant proteins		
Alexa Fluor™ 568 Hydrazide	ThermoFisher	A10437
Neurobiotin Tracer	Vector Laboratories	SP-1120
ChemiBLOCKER	Millipore	2170
Triton X-	Sigma Aldrich	X102
Streptavidin Cy5	ThermoFisher	SA1011
Experimental models: Organisms/strains		
C57BL/6J Cx36KO	Deans et al., 2001[106]	N/A
Thy1-GCaMP3	The Jackson Laboratory	JAX 017893
Software and algorithms		
Axoscope	Molecular Devices	Molecular Devices Axoscope
BrainWave 4	3Brain	Brainwave 4
Fiji/ImageJ	Schindelin et al., 2012[107]	https://fiji.sc
Hearding-Spikes	Hilgen et al., 2017[108]	https://pypi.org/project/herdingspikes/
Kneed	Satopaa et al., 2011[109]	https://pypi.org/project/kneed/
McRack	Multichannel systems	McRack
Neuroexplorer	Plexon	Neuroexplorer
Offline Sorter	Plexon	Offline Sorter
OriginPro 18	Origin Lab	https://www.originlab.com/
Psychopy	Peirce et al., 2019[110]	https://www.psychopy.org/
Scikit-learn	Pedregosa et al., 2012[111]	https://pypi.org/project/scikit-learn/
WinWCP	University of Strathclyde	WinWCP
Other		
60 Channel MEA	Multichannel systems	60MEA100/10iR-Ti
Arena HD-MEA	3Brain	Arena HD-MEA
Carbostar-1 CF microelectrode	Kation Scientific	E1011-7
Glass Capillaries	World Precision Instruments (WPI)	1B150F-4

RESOURCE AVAILABILITY

Lead contact

Further information and requests for resources and reagents should be directed to and will be fulfilled by the lead contact, Béla Völgyi (volgyi01@gamma.ttk.pte.hu).

Materials availability

This study did not generate new unique reagents.

Data and code availability

- Data reported in this paper will be shared by the lead contact upon request.
- This paper does not report original code.
- Any additional information required to reanalyze the data reported in this paper is available from the lead contact upon request.

EXPERIMENTAL MODEL AND SUBJECT DETAILS

Adult male or female (P30-90) C57BL6J (n = 29), connexin 36 knock-out (Cx36 KO) on C57BL6J background (n = 7) and Thy1-GCaMP3 (n = 12) (JAX, Strain #:017893) mice were used in this study. After overnight dark adaptation, animals were put under deep anesthesia using Forane (4%, 0.2 mL/L) inhalation and terminated through cervical dislocation. Dissection and experimentation were carried out in mammalian Ringer's solution (125 mM NaCl, 3 mM KCl, 2 mM CaCl$_2$, 1.0 mM MgCl$_2$, 25 mM NaHCO$_3$, 1.25 mM NaH$_2$PO$_4$, 10 mM glucose, pH 7.4[112]) under dim red illumination. The eyes and the retina were removed and hemisected anterior to the ora-serrata. In the single-cell extracellular recordings carried out with tungsten microelectrodes, anterior optics and the vitreous humor were removed, and the resultant retina-eyecup was placed in a superfusion chamber. In MEA or patch clamp (PC) experiments, the retina was completely isolated from the eyecup and attached directly atop the array or a filter paper (Millipore) to further transfer under the PC electrophysiology setup. All animals were treated in accordance with the ARVO Statement for the Use of Animals in Ophthalmic and Vision Research. Maintenance and animal housing were all carried out in accordance with the local Animal Welfare Committee guidelines and regulations (University of Pécs, BA02/2000-6/2006; BA/35/ 51-42/2016; BA/73/00504-5/2021). All efforts were made to minimize pain and discomfort.

METHOD DETAILS

Extracellular electrophysiology

Single-cell extracellular recordings were obtained from RGCs using tungsten microelectrodes (1MΩ; Kation Scientific LCC Minneapolis, MN, USA), an AC differential amplifier (DAM80i, World Precision Instruments) and an analog-to-digital board (Digidata 1440a; Axon Instruments, Sunnyvale, CA, USA). Spiking activity was recorded digitally at a sampling rate of 20 kHz with Axoscope (Axon Instruments, Foster City, CA). In a second set of experiments, 60 and 120 channel MEA systems (Multi Channel Systems MCS GmbH, Reutlingen, Germany) were used to detect RGC spiking activity and recordings were made using the MCRack software (Multi Channel Systems MCS GmbH, Reutlingen, Germany). In a third cohort of experiments a BioCAM-X high density multielectrode (HD-MEA; 4096 channels) system and the BrainWave software was used for data acquisition (3Brain AG, Zürich, Switzerland). In pharmacology experiments picrotoxin (PTX; 50 μM), meclofenamic acid (MFA; 20, 40, and 80 μM), Quinine (100 μM) and L-2-amino-4-phosphonobutyric acid (APB; 50 μM) were applied separately and independently.

Patch clamp recordings, dye injections

Patch clamp (PC) recordings were performed with an Axopatch 200B PC amplifier (Axon Instruments Inc., Union City, CA, USA) and ECS-filled PC pipettes (≈ 20 MΩ; borosilicate glass, 1.5/0.84 mm ID/OD, WPI) in loose patch configuration (voltage clamp mode). Signals were digitized with a Digidata 1440A ADC (Axon Instruments, Inc.) and acquired with WinWCP software (John Dempster, University of Strathclyde, Glasgow, UK). Electrodes used for dye staining and stimulation were filled with intracellular solution (ICS; 20–30 MΩ borosilicate glass pipettes, 1.5/ 0.84 mm ID/OD, WPI). Electrodes were pulled with a P-87 micropipette puller (Sutter Instruments, Novato, CA, USA). The ICS contained 125 mM potassium gluconate, 8 mM NaCl, 0.6 mM MgCl$_2$, 1 mM EGTA, 10 mM HEPES, 2 mM Mg-ATP, and 0.4 mM Na-GTP at pH 7.3 (KOH adjusted) and was supplemented with a combination of 0.5% A568-hydrazide and either 4% Neurobiotin (NB) or 0.1% serotonin[51] to fill target cells via electroporation [NB: +65 mV pulses at 1 Hz (V = −50 mV; R = 90 MΩ); serotonin: −65 mV pulses at 1 Hz (V = 15 mV; R = 90 MΩ)]. In the PC recordings, the pharmacological agents were added to the Ringer solution and loaded into the Patch pipette.

Light stimulation

In the extracellular recordings, a uniform full-field stimulus was used to evoke light responses (0.5 s illumination every 2 s). In experiments utilizing different stimulus intensity of light stimuli values were given in terms of the rate of photoisomerization that occurs in each rod in every second (Rh*/rod/s); we calculated with an average rod density of 437,000 rods/mm2[113] and quantum efficiency of 0.67.[114] The intensity of the light stimuli varied from 1 to 6000 Rh*/rod/sec. For the Patch clamp recordings light stimuli patterns were programmed in the PsychoPy free cross-platform software[110] and were then delivered by a high-definition LED projector through an ND2 filter and directly focused on the surface of the retina. To verify the identity of the transient OFF alpha cells, full-field and approaching stimuli were utilized. For full-field stimuli, full-field white (gray value - gv: 256) and black illumination (gv: 0) were alternated (cycle: 1 s, with 0.5 s white illumination and 0.5 s black illumination). For the approaching stimuli, a 40 μm black circle was projected over soma for 1 s. The diameter was then increased from 40 μm to 240 μm in 0.5 s (400 μm/s).

Data analysis

In general spike sorting was carried out using Spike2 (CED, Cambridge, UK) and Offline Sorter (Plexon Instruments, Dallas, TX, USA), whereas for the HD-MEA recordings Hearding-Spikes sorter was utilized.[115] Peristimulus time histograms (PSTH) measuring transiency were generated

in NeuroExplorer (Plexon Instruments, Dallas, TX, USA) or through a Python script utilizing the Scikit-learn package.[111] Gaussian smoothing (filter size: 3) was applied to all datasets. All transiency values were calculated using the PSTHτ method,[18] where PSTHτ measures the time required for spiking frequency to decrease to 1/e of the peak firing amplitude. As selective GJ blockers to target GJs in the circuitry are not available we utilized bimodal and/or unimodal peaks in cross-correlation functions (CCFs) generated upon RGC pair recordings to identify and separate RGCs with RGC-RGC and RGC-AC GJ connections that display bimodal and narrow unimodal CCF peaks, respectively.[43] CCFs were calculated based on the Python NumPy correlation coefficient for bins of 1 ms and visualized using Matplotlib. The peaks were detected, thereby categorizing the CCFs into bimodal and unimodal CCF peaks. Subsequently, the inflexion points of the CC graphs were determined using the KneeLocator function of the KNEED module, splitting the unimodal CCFs into narrow (<50 ms) and wide (>50 ms) categories. SPSS (v19, IBM, Armonk, NY, USA).

Post hoc histochemistry

To visualize NB-filled cells, samples were incubated for a minimum of 30 min. Tissues were then fixed in 4% paraformaldehyde solution for 15–25 min, washed with phosphate buffered saline (PBS), and blocked with CTA (5% Chemiblocker, 0.5% Triton X-100, 0.05% sodium azide in PBS) overnight, then incubated in Streptavidin Cy5 (Thermo Fisher Scientific; 1,500x dilution) in CTA overnight. Samples with serotonin-filled cells were processed for serotonin immunohistochemistry by applying anti-serotonin antiserum (Sigma-Aldrich, St. Louis, MO, USA, catalog number: S5545, 2,000x dilution) for 2 days and, following a thorough washing (4x in PBS), adding DyLight 405 AffiniPure Goat Anti-Rabbit (111-475-003, 500x) secondary serum to the tissue for fluorescent visualization. Washed retina samples were placed on slides mounted in VectaShield (Vector Laboratories, Newark, CA, USA) and cover-slipped for microscopy. In addition to tracer visualization, we also performed other immunohistochemistry experiments with the same protocol as the serotonin labeling for rabbit choline acetyltransferase (ChAT; ThermoFisher, PA5-29653, 1,500x) and rabbit hyperpolarization-activated cyclic nucleotide-gated potassium channel 4 (HCN4; Alomone Labs, Jerusalem, Israel; APC-052, 1,500x).

Confocal microscopy and image processing

Retinal samples were scanned with a Zeiss LSM710 confocal microscope with 20x (Z = 1 μm; Zeiss W Plan-Apochromat 20/1.0×) and 63× objectives (Z = 0.5 μm; Zeiss Plan Apochromat 63/1.4) at high resolution and normalized laser intensity. Minor manipulations of brightness and contrast of images were performed in FIJI – ImageJ, NIH, and Adobe Photoshop CC (Adobe Systems Inc., San Jose, CA, USA).

Injected cell array reconstructions

Confocal z-stacks were imported into FIJI. After utilizing the Simple Neurite Tracer[116] plugin, all paths of each cell were traced. First, the soma was traced in concentric circles from the first to last virtual section in which it was present, then, originating from the soma path, further paths were traced to the upcoming intersection until the whole dendritic arbor was selected. Having selected all the paths belonging to each cell, the fill-out feature was performed, and the fill was exported as a grayscale image. The grayscale images were used for further analyses and, using the FIJI three-dimensional (3D) viewer plugin, 3D models were generated for visualization.

QUANTIFICATION AND STATISTICAL ANALYSIS

OriginPro 18 (Origin Lab Corp., Northampton, MA, USA) was used for statistical analysis. Shapiro-Wilk normality test was performed to determine normal distribution. When normal distribution was assumed paired t-test was used, otherwise Wilcoxon signed ranks test was utilized as a non-parametric test. Statistical significance was assumed under $p = 0.5$ (*), on all figures are displayed as means $\pm$ standard deviation and statistical significance was reported as * $p < 0.05$ and *** $p < 0.001$. Statistical results are shown both in the Results and the respective Figure legends. The definition of n-values are stated in the corresponding Result paragraph.